Accepted Manuscript

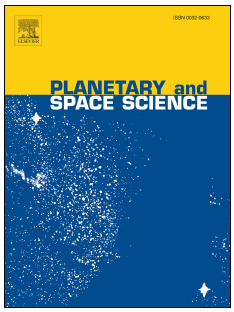

The science process for selecting the landing site for the 2020 Mars rover

John A. Grant, Matthew P. Golombek, Sharon A. Wilson, Kenneth A. Farley, Ken H. Williford, Al Chen

PII: S0032-0633(18)30107-7

DOI: 10.1016/j.pss.2018.07.001

Reference: PSS 4572

To appear in: *Planetary and Space Science*

Received Date: 13 March 2018

Revised Date: 8 June 2018

Accepted Date: 1 July 2018

Please cite this article as: Grant, J.A., Golombek, M.P., Wilson, S.A., Farley, K.A., Williford, K.H., Chen, A., The science process for selecting the landing site for the 2020 Mars rover, *Planetary and Space Science* (2018), doi: 10.1016/j.pss.2018.07.001.

The Science Process for Selecting the Landing Site for the 2020 Mars Rover

John A. Grant[a], Matthew P. Golombek[b], Sharon A. Wilson[a], Kenneth A. Farley[c], Ken H. Williford[b], Al Chen[b].

[a]Center for Earth and Planetary Studies, National Air and Space Museum, Smithsonian Institution, 6th at Independence SW, Washington, DC, 20560,
[b]Jet Propulsion Laboratory, California Institute of Technology, 4800 Oak Grove Drive, Pasadena, CA, 91109,
[c]Division of Geological and Planetary Sciences California Institute of Technology, Pasadena, CA 91125 Pasadena, CA 91125

Abstract

The process of identifying the landing site for NASA's Mars 2020 rover began in 2013 by defining threshold mission science criteria related to seeking signs of ancient habitable conditions, searching for biosignatures of past microbial life, assembling a returnable cache of samples for possible future return to Earth, and collecting data for planning eventual human missions to the surface of Mars. Mission engineering constraints on elevation and latitude were used to identify candidate landing sites that addressed the scientific objectives of the mission. However, for the first time these constraints did not have a major influence on the viability of candidate sites and, with the new entry, descent, and landing capabilities included in the baseline mission, the vast majority of sites were evaluated and down-selected on the basis of science merit. More than 30 candidate sites with likely acceptable surface and atmospheric conditions were considered at a series of open workshops in the years leading up to the launch. During that period, iteration between engineering constraints and the evolving relative science potential of candidate sites led to the identification of three final candidate sites: Jezero crater (18.4386°N, 77.5031°E), northeast (NE) Syrtis (17.8899°N,77.1599°E) and Columbia Hills (14.5478°S, 175.6255°E). The final landing site will be selected by NASA's Associate Administrator for the Science Mission Directorate. This paper serves as a record of landing site selection activities related primarily to science, an inventory of the number and variety of sites proposed, and a summary of the science potential of the highest-ranking sites.

1. Introduction

The Mars 2020 rover and its payload of seven science instruments will evaluate surface materials to achieve the science objectives established by the National Aeronautics and Space Administration (NASA). These include: exploration of an ancient astrobiologically relevant environment that preserves information to constrain the geological record, including past habitability and biosignature preservation potential; searching for potential biosignatures; and caching samples for possible future return to the Earth (Farley and Williford, 2017) (Table 1).

Table 1. Overarching science objectives of the Mars 2020 Mission*

Science Objectives	
Conduct Rigorous In Situ Science	**Enable the Future**
Geology: Characterize the processes that formed and modified the geologic record within a field exploration area on Mars selected for evidence of an astrobiologically relevant ancient environment and geologic diversity.	*Potential Sample Return*: Collect scientifically selected samples, for which the field context is documented, that contain the most promising astrobiologically relevant samples, and that represent the geologic diversity of the field site.
Astrobiology: Determine the habitability of an ancient environment, search for materials with high biosignature preservation potential, and search for potential evidence of past life.	*Human Exploration/Technology*: Contribute to the preparation for human exploration of Mars by making significant progress towards filling at least one major Strategic Knowledge Gap.

*From the Mars 2020 Science Definition Team (Mustard et al., 2013) and Mars 2020 Announcement of Opportunity (NASA 2013).

Rigorous selection of a landing site for the 2020 rover plays a crucial role in the success of the mission because it guides the rover to a location on Mars where the science objectives can be best achieved. This paper emphasizes activities related to the assessment of the science merit for each proposed 2020 landing site against scientific criteria derived from the mission science objectives (Table 2). This process was informed by an unprecedented variety of orbital datasets from multiple instruments across a number of Mars missions that were synthesized to

64 characterize each candidate landing site from the standpoint of science and safety. The objective
65 of all landing site activities is to maximize the probability of landing safely with access to high-
66 priority science targets. Because the rover and "sky crane" entry, descent, and landing (EDL)
67 system are evolved from those of the preceding Mars Science Laboratory (MSL) *Curiosity* rover
68 (Bernard and Farley, 2016), many of the engineering constraints are comparable (Table 3). The
69 higher atmospheric density expected on arrival at Mars in 2021 (Golombek et al., 2015) and
70 inclusion of new EDL navigational capabilities on the 2020 rover (Golombek et al., 2015, 2016;
71 Coombs, 2016; Farley and Williford, 2017), however, enables a smaller landing ellipse at higher
72 elevation and provides access to locales where surface relief precluded landing by *Curiosity*
73 (Table 3).

74 **Table 2**. Science criteria used to evaluate potential 2020 landing sites*. Potential landing sites
75 must meet the threshold geological criteria and potential qualifying geological criteria will help
76 rank sites meeting the threshold criteria.
77

Threshold Geologic Criteria
Presence of subaqueous sediments or hydrothermal sediments (equal 1st priority), OR Hydrothermally altered rocks or low-temperature fluid-altered rocks (equal 2nd priority)
Presence of minerals indicative of aqueous phases (e.g., phyllosilicates, carbonates, sulfates, etc.) in outcrop
Noachian/Early Hesperian age based on stratigraphic relations and (or) crater counts
Presence of igneous rocks of any age, to be identified as primary materials
Not a Special Region (water or ice within 1m of surface) for planetary protection
Potential Qualifying Geologic Criteria (in order of importance)
Morphological criteria for standing bodies of water and (or) fluvial activity (deltaic deposits, shorelines, etc.)
Assemblages of secondary minerals of any age (e.g., reflecting multiple phases of activity)
Presence of former water ice, glacial activity or its deposits
Igneous rocks of Noachian age, known stratigraphic relation, better if includes exhumed megabreccia
Volcanic unit of Hesperian or Amazonian age well defined by crater counts and well-identified by morphology and (or) mineralogy
Probability of samples of opportunity (ejecta breccia, mantle xenoliths, etc.)
Potential for resources for future human mission

78 *Based on findings of the E2E-iSAG (McLennan et al., 2011) and the Mars 2020 Science
79 Definition Team (Mustard et al., 2013)
80

Table 3. Summary of landing site engineering constraints and safety criteria for the Mars 2020 rover developed during Phase A of the mission (Fiscal Year 2014)

Engineering Parameter	**Requirement for Landing Sites**	**Notes/Rationale**
Latitude	30°N to 30°S	Sites poleward of 30°N and 30°S have surface thermal limitations
Elevation	< -0.5 km[+]	Relative to the Mars Orbiter Laser Altimeter (MOLA) datum
Radius and Azimuth of Landing Ellipse	≤ 16.0 km (down-track direction, approx. W-E) 14 km (cross-track direction, approx. N-S)[@]	Using range trigger reduces the ellipse size, includes wind-induced uncertainty during parachute descent
Terrain Relief/Slopes	2–10 km length scale: ≤ 20°	Radar spoofing in preparation for powered descent[*]
	1–2 km length scale: ≤ 43 m relief at 1 km, linearly increasing to 720 m and 2 km[*]	Radar spoofing in preparation for powered descent[*]
	1 m to 1000 m baseline length scale: ≤ 100 m relief	For control authority and fuel consumption, increased from MSL
	2 m to 5 m length scale: ≤25°-30°	Rover landing stability/trafficability after landing; Increased from original MSL specification
Rock Height	≤ 0.6 m (assumes a max rock height of 0.55 m and a rover sinkage of 0.05 m)	< 0.50% probability rock > 0.6 m high occurs in random area of 4 m^2 (belly pan) (~12% rock abundance)[*]
Radar Reflectivity	Ka band reflective	Adequate Ka band radar backscatter cross-section (> -20 dB and < 15 dB)[*]
Load Bearing Surface	Not dominated by dust	Thermal inertia > 100 J m-2 s -0.5 K-1 and albedo <0.25; radar reflectivity >0.01 for load bearing bulk density[*]
Atmosphere	Up to 25 m/s horizontal and 20 m/s vertical winds	During EDL[*]
Surface winds for Thermal Environment	During Operation: < 15 m/s (steady) < 30 m/s (gusts) Non-Operation (sleeping): <40 m/s (steady)	For 1 m above the surface. These constraints provide an environment in which the rover can perform science operations[*]
[*] Same as MSL *Curiosity*		
[+] Updated in October, 2014 from original requirement of ≤ +0.5 km		
[@] Updated in March, 2015 from original requirement of 25 km x 20 km		

Science and engineering assessment and characterization of the candidate landing sites emphasizes data from the Mars Reconnaissance Orbiter (MRO) Compact Reconnaissance Imaging Spectrometer for Mars (CRISM) (Murchie et al., 2007), High Resolution Imaging Science Experiment (HiRISE) (McEwen et al., 2007), and Context Camera (CTX) (Malin et al., 2007) instruments. Data from the Mars Odyssey Thermal Emission Imaging System (THEMIS) (Christensen et al., 2004) instrument, Mars Global Surveyor (MGS) Mars Orbiter Camera (MOC) (Malin et al., 1992) and Mars Orbiter Laser Altimeter (MOLA) (Zuber et al., 1992), Mars Express Observatoire pour la Minéralogie, l'Eau, les Glaces et l'Activité (OMEGA) (Bibring et al., 2004) spectrometer, and High Resolution Stereo Camera (HRSC) (Jaumann et al., 2007) were also utilized. Data from the Mars Climate Sounder (MCS) (McCleese et al., 2007) and the Mars Color Imager (MARCI) (Bell et al., 2009) on MRO were emphasized in atmosphere characterization related to the engineering assessment of the candidate sites.

A key element of the MRO imaging plan for candidate landing sites involved rapid release of data to scientists to expedite the evaluation of the relative merits and risks of proposed sites, thereby making data documenting scientifically interesting locations on Mars available to the science community before their regular release date. Assessment of the sites also depended on the work of investigators funded by NASA's Mars Data Analysis Program and the Mars Exploration Program's Critical Data Analysis Program (CDP) to provide key higher-level data products that enabled characterization of sites (e.g., rock abundance, surface properties, and relief).

The safe delivery of the 2020 rover to Mars' surface also depends upon the characterization of the atmosphere through which the spacecraft descends. The spacecraft's EDL system involves a guided entry, parachute deployment, and a rocket-powered terminal descent to the surface

(Bernard and Farley, 2016). A team of atmospheric scientists advised the mission and provided model-based predictions of atmospheric density, winds, and the probabilities and possible effects of dust storms during the 2020 rover arrival season. Moreover, planetary protection considerations warrant the exclusion of "special regions" where liquid water may exist at the surface (e.g., recurring slope lineae (RSL) (McEwen et al., 2014)), where there is evidence for water or ice within 1 m of the surface (Rummel et al., 2014; Golombek et al., 2015), or possibly other induced special regions (e.g., Shotwell et al., 2017). These atmospheric and planetary protection assessments are described in separate publications (e.g., Shotwell et al., 2017), whereas this manuscript focuses mostly on the terrain.

The inferred geologic setting of the site must lend confidence that the rocks and outcrops are available, accessible, and suitable for achieving core science objectives (Table 1) (Mustard et al., 2013; Farley and Williford, 2017). While both science and engineering aspects of landing site selection are critical to mission success, the engineering constraints trump science because there is no science return unless the mission lands safely on the surface of Mars.

Due to the diverse nature and growing quantity of data available for interpretation of the Martian surface, the broad expertise of the Mars science community was enlisted to assist in the landing site selection process via proposal and assessment of candidate sites at a series of workshops that were open to the science community and public. The process is modeled after the successful Mars Exploration Rover (MER) *Spirit* and *Opportunity* (Golombek et al., 2003; Grant et al., 2004) and *Curiosity* (Grant et al., 2010a; Golombek et al., 2012) site selection processes.

Cooperation between the Mars 2020 science and engineering teams (hereafter referred to as the "2020 Project" or "Project") and the science community is essential to the success of the process and is accomplished in part via oversight by a NASA-appointed Mars Landing Site

Steering Committee (Table 4). The Committee, co-chaired by a member of the Mars Exploration Program Office at the Jet Propulsion Laboratory (JPL) (Dr. Matthew Golombek) and a member of the science community (Dr. John Grant), includes additional members of the science community with a range of scientific expertise (Table 4). Recognition of the need to involve additional scientists and engineers not on the Committee in the process, possessing experience in past and ongoing missions and site characterization and selection, led to solicitation of, and participation by, a variety of people in the science community and at NASA. Expertise on returned samples was incorporated via a NASA and Mars 2020 Project appointed Returned Sample Science Board (RSSB) comprised of scientists that included both Mars and non-Mars experts (Table 5). In addition, the co-chairs of the Landing Site Steering Committee worked closely with NASA Headquarters, the MRO Project, and the Mars 2020 Project to define the number and rate at which MRO data of candidate landing sites were targeted and obtained.

Table 4. NASA appointed Mars 2020 rover landing site Steering Committee

Name	**Role**	**Affiliation**
John Grant	Co-Chair	Smithsonian Institution
Matthew Golombek	Co-Chair	Jet Propulsion Laboratory
Dave Desmarais	Member	NASA Ames Research Center
Brad Jolliff	Member	Washington University St. Louis
Scott McLennan	Member	SUNY Stony Brook
John Mustard	Member	Brown University
Steve Ruff	Member	Arizona State University
Kenneth Tanaka	Member	U.S. Geological Survey, Flagstaff

Table 5. NASA and Mars 2020 Project appointed Returned Sample Science Board (RSSB)

Name	**Role**	**Affiliation**
David Beaty	Co-chair	Jet Propulsion Laboratory
Hap McSween	Co-chair	University of Tennessee
Andrew Czaja	Member	University of Cincinnati

Elizabeth Hausrath	Member	University of Nevada
Chris Herd	Member	University of Alberta
Munir Humayun	Member	Florida State University
Scott McLennan	Member	Stony Brook University
Lisa Pratt	Member	Indiana University
Mark Sephton	Member	Imperial College
Andrew Steele	Member	Carnegie Institute of Washington
Ben Weiss	Member	Massachusetts Institute of Technology
Francis McCubbin	Ex officio	NASA Johnson Space Center
Yulia Goreva	Ex officio	Jet Propulsion Laboratory
Michael Meyer	Observer	NASA Headquarters
Betsy Pugel	Observer	NASA Headquarters
Lindsay Hays	Observer	Jet Propulsion Laboratory

The Steering Committee helps to ensure the process includes the broader science community, remains focused on criteria appropriate for site assessment, stays on schedule for key Project decisions, and that workshop discussions emphasize candidate sites with the highest science potential. Activities include advertising requests to propose candidate sites, convening open community workshops where the science merit of candidate sites is discussed, and helping to ensure that all relevant data are made available and used in the proposal, consideration, and selection of candidate sites. The science community, via the Steering Committee, provides assessment of the relative potential merits of candidate sites to the Project, which then recommends one or more sites to NASA where the final site is ultimately selected by NASA's Associate Administrator for the Science Mission Directorate.

The science community and NASA are updated on the Mars 2020 site selection process via presentations at professional conferences (e.g., Golombek et al., 2015, 2016, 2017, 2018), Mars Exploration Program Assessment Group (MEPAG) meetings, and briefings to NASA Headquarters personnel. These presentations also serve to advertise upcoming community

workshops. In addition, summaries of all activities, workshops, and workshop presentations are available online through a JPL website: https://marsnext.jpl.nasa.gov.

2. Beginning the Process of Selecting the Landing Site for Mars 2020

Landing site selection activities began in earnest in 2013 with publication of the report of the Mars 2020 Science Definition Team (SDT) (Mustard et al., 2013), followed by definition of the initial mission engineering constraints (Table 3) and the first call for candidate landing sites. The initial call in late 2013 intended to get a jump start on the imaging of locations with high science interest using MRO instruments to enable robust assessments and mature discussions of the potential merits and shortcomings for the broadest possible set of sites (relative to both engineering and science constraints) during the first landing site workshop. This call yielded nine pre-Workshop 1 ("Pre-W1") sites (Table 6), which built upon an existing database of 55 candidate landing sites previously proposed post-MSL and pre-2020 for a wide range of more generic future mission scenarios (some were not appropriate for the 2020 mission due to a poor match to engineering constraints and (or) targeted science objectives). Collectively, 30 unique HiRISE targets (many were stereo requests) and 27 CRISM were requested and images began to be acquired of these nine candidate sites in advance of the first Mars 2020 landing site workshop.

180

181 **Table 6.** Candidate Mars 2020 Rover landings sites proposed and discussed at the first landing site workshop. The final 8 sites are

182 shaded grey.

Location[a]	Site Name[b]	Center of Proposed Nominal Ellipse			Proposed Science Target(s)	Site Advocate(s)[c]	Proposed[d]	Rank at end of W1	Rank at end of W2	Post W2: Sites considered at W3	Post W3 Sites
		Lat. (°N)	Lon. (°E)	Elev. (km)							
1	Southwestern Melas basin	-9.81	283.53	-1.92	Paleolake setting with lacustrine deposits, submarine fans, shallow deltas. Also alluvial fans, fluvial valleys, debris flows, landslides, layered deposits, volcanic ash, hydrated silica and sulfates	**R. Williams**, C. Weitz, C. Quantin-Nataf, G. Dromart, P. Grindrod, J. Davis, P. Thollot, L. Mandon, L. Edgar	W1, W2, W3	7	5	selected among final 8	---
2	East Melas Chasma	-12.22	290.09	-4.23	Layered deposits of unknown origin, includes landslides consisting of Hesperian volcanics and phyllosilicates	**S. Turner**, J. Bridges, S. Grebby	Pre-W1	24	---	---	---
		-11.47	291.48	-4.8	Layered deposits of unknown origin, hydrated sulfates, phyllosilicates, recurring slope lineae (RSL)	**H. Miyamoto**, G. Komatsu, A. McEwen, M. Chojnacki, T. Usui, A. Yamagishi	W1				
3	Coprates Chasma	-12.6	296.1	-5	Primitive crustal materials including phyllosilicates, volcanics, sulfates, and layered deposits with possible aqueous depositional signatures	**C. Quantin-Nataf**, B. Bultel, J. Flahaut, P. Thollot, J. Carter, A. Ody, D. Loizeau, L. Lozac'h, M. Andreani, I. Daniel, H. Clenet	W1, W2	20	15	---	---
4	Juventae Chasma	-4.39	298.42	-3.1	Interior layered deposits, sulfate mounds, possible volcanics, RSL	**H. Miyamoto**, G. Komatsu, A. McEwen, M. Chojnacki, T. Usui, A. Yamagishi	W1	26	---	---	---
5	Capri Chasma	-15.23	309.5	-4.45	Phyllosilicates of unknown origin, RSL, volcanics	**H. Miyamoto**, G. Komatsu, A. McEwen, M. Chojnacki, T. Usui, A. Yamagishi	W1	25	---	---	---
6	Vistula Valles/Chryse	14.6	309.6	-2.6	Fluvial sedimentary and other sedimentary rocks possibly emplaced in water, capped by regional lava flow.	**K. Edgett**, L. Saper	Pre-W1	---	---	---	---
7	Sabrina delta	11.99	313.4	-2.62	Delta stratigraphy,	**T. Platz**, E. Hauber, L. Le Deit,	W1, W2	21	20	---	---

	(Magong crater)				phyllosilicates, opaline silica, tephra deposits, dykes	S. van Gasselt, K. Kinch, M. Madsen, H. Rosenberg					
8	Hypanis delta (Xanthe Terra)	11.91	314.64	-2.63	Delta stratigraphy, phyllosilicates, hydrated minerals	**S. Gupta**, P. Fawdon, P. Grindrod, M. Balme, E. Hauber, J. Carter, A. Dumke, S. van Gasselt, J-P. Muller, J. Michalski, S. Sidiropoulo, E. Sefton-Nash, J. Davis, N. Warner	W1, W2	17	11	---	---
9	Holden crater	-26.61	325.18	-2.18	Alluvial fans and layered fluvial and lacustrine phyllosilicate-bearing materials, ancient impact megabreccia	**R. Irwin**, J. Wray, J. Grant, A. Anglés, M. Pondrelli, G. Caprarelli, E. Jones, D. Flannery, R. Orosei, M. Walter, C. Lineweaver	W1, W2, W3	5	9	selected among final 8	
10	Eberswalde crater	-23.77	326.49	-1.49	Fluvial, deltaic, and lacustrine deposits. Deposits include phyllosilicates, alluvial fan delta, channels, and impact megabreccia	**R. Irwin**, M. Rice, N. Warner, S. Gupta, J. Adler	W1, W2, W3	11	4	selected among final 8	
11	Ladon Valles	-20.06	329.9	-2.069	Layered light toned phyllosilicate-bearing, detrital material eroded from upstream Noachian/Hesperian outcrops, also volcanic flows	**C. Weitz**, J. Bishop, J. Grant	W1, W2	12	13	---	---
12	Oxia Planum	17.8	336	-3.02	Noachian basement material including layered deposits, fluvial valleys and channels, delta-fan, phyllosilicates, hydrated silica, carbonates, and lava flows	**P. Thollot**, C. Quantin-Nataf, J. Carter, D. Loizeau, B. Bultel, L. Lozach, J. Davis, P. Grindrod, J. Fernando, M. Pajola, J. Broyer, E. Baratti, R. Sandro, P. Allemand, C. Leyrat, A. Ody	W1, W2	14	19	---	---
13	McLaughlin crater	21.9	337.8	-5.03	Layered deposits with phyllosilicates, carbonates, associated with groundwater source and (or) lacustrine environment	**J. Michalski**, F. Chuang, P. Niles, S. Johnson, J. Mustard, J. Bishop, J. Bleacher, C. Cockell, D. Dyar, A. Fairén, J. Farmer, T. Glotch, V. Hamilton, B. Hynek, T. Kieft, A. McAdam, T. McCollom, A. McEwen, E. Noe Dobrea, T. Onstott, J. Parnell, D. Rogers, M. Russell, E. Shock, J. Stern, S. Van	W1, W2	6	10	---	---
14	Oyama crater	23.41	340.19	-3.877	Fluvial sediments derived from adjacent Mawrth Vallis plateau, phyllosilicate-bearing layered deposits, and lava	**D. Loizeau**, N. Mangold, J. Michalski, J. Bishop, J. Carter, S. Werner, F. Poulet	W1, W2	10	16	---	---

					flows.						
15	Mawrth Vallis	23.97	340.94	-2.24	Noachian layered deposits of unknown origin, but with diverse phyllosilicates, sulfates and other aqueous alteration minerals and widely exposed in aligned mesas, inverted channels, numerous fractures and veins. Igneous rocks.	**D. Loizeau**, N. Mangold, J. Michalski, J. Bishop, J. Carter, S. Werner, **B. Farrand**, J. Rice, E. Noe Dobrea, J. Michalski, F. Chung, F. Poulet, B. Horgan	W1, W2, W3	8	8	selected among final 8	---
16	Kashira crater	-27.37	341.58	-0.375	Crater with inlet/outlet channels, shoreline morphologies, and Kaolin-bearing central mound. Light-toned material of unknown origin and volcanic plains	**M. Salvatore**, T. Goudge, J. Mustard, J. Head	Pre-W1, W1	18	---	---	---
17	Intercrater West Arabia	19.9	343	-2.03	Inverted fluvial channels and associated lacustrine, light-toned phyllosilicate-bearing rocks bounded by cratered highlands bedrock	**K. Edgett**, L. Saper	Pre-W1	---	---	---	---
18	Firsoff crater	3.13	350.68	-2.743	Equatorial layered deposits, of unknown origin that include hydrous minerals (sulfates), possible spring deposits, mud volcanos, and ridges.	**M. Pondrelli**, A. Rossi, B. Cavalazzi, F. Fueten, M. Glamoclija, E. Hauber, L. Le Deit, S. van Gasselt, T. Zegers, F. Franchi	Pre-W1, W1	23	---	---	---
19	Farthest West Meridiani	-0.7	351.8	-1.96	Meridiani "Burns Formation" rocks above a lava flow that overlies possible inverted channels. Wind-eroded yardangs (in sedimentary rocks)	**K. Edgett**, L. Saper	Pre-W1	---	---	---	---
20	East Margaritifer Terra	-5.64	353.87	-1.22	Ancient fluvial and lacustrine setting that includes phyllosilicates, chlorides (exposed detrital and evaporitic sedimentary deposits) and capping basaltic material.	**P. Christensen**, M. Salvatore, V. Hamilton, C. Edwards, T. Onstott, C. Cockell, T. Lowenstein, L. Ziolkowski, N. Tosca, J. Huang	W1, W2	9	14	---	---
21	Meridiani Planum	-2.06	354.01	-1.3	Sulfate plains, Noachian phyllosilicates	**M. Golombek**	W1	27	---	---	---
22	Northwest Hellas	-26.14	56.43	-0.7	Sedimentary layers of possible aqueous origin forming pitted plains, with phyllosilicates	**E. Noe Dobrea**, S. Mest, F. Chuang, J. Mustard, D. Crown, G. Swayze	W1	19	---	---	---

					and other alteration minerals.						
23	Leighton crater	3.0	57.5	0.31	Rocks displaying textures possibly consistent with a hydrothermal origin and containing carbonates.	**J. Michalski**, F. Chuang, P. Niles, J. Mustard, J. Bishop, J. Bleacher, C. Cockell, D. Dyar, A. Fairén, J. Farmer, T. Glotch, V. Hamilton, B. Hynek, T. Kieft, A. McAdam, T. McCollom, A. McEwen, E. Noe Dobrea, T. Onstott, J. Parnell, D. Rogers, M. Russell, E. Shock, J. Stern, S. Van	W1	---	---	---	---
24	Nili Patera	9.07	67.4	0.208	Putative hydrothermal silica deposits and surrounding volcanic rocks	**J. Skok**, P. Fawdon, S. Karunatillake, J. Mustard, C. Fassett	Pre-W1, W1	15	18	---	---
25	Nili Fossae (South)	19.7	73.8	-0.41	Outcrops possibly formed in an ancient hydrothermal setting that are carbonate- and phyllosilicate-bearing near volcanic materials. , Morphologies include a possible fan or debris flow and impact megabreccias.	**C. Viviano-Beck**, A. Brown, E. Amador, J. Mustard, K. Cannon	W2	---	12	---	---
26	Nili Fossae	21.03	74.35	-0.65	Noachian rocks that include phyllosilicates, clay-rich ejecta and impact melt-bearing rock from Hargraves crater, and adjacent Hesperian volcanics	**J. Mustard**, B. Ehlmann, K. Cannon, N. Mangold, S. Parman, D. Des Marais, C. Edwards, E. Amador, J. Skok, F. Poulet, L. Tornabene, H. Sapers, A. Brown, G. Osinski, H. Sare, C. Ryan, A. Pontefract, A. Bina, C. Cockell	W1, W2, W3	2	6	selected among final 8	---
27	Nilosyrtis crater	27.97	74.73	-0.55	Fluvio-lacustrine landforms (including linear ridge networks) and sediments that display a smectite-kaolinite-jarosite- bearing stratigraphy.	**L. Saper**	Pre-W1	---	---	---	---
28	Northeast Syrtis	17.8899	77.1599	-2.04	Diverse rock assemblage with likely weathering zones. Includes mafic rocks, olivine-rich carbonate rocks, Noachian layered phyllosilicate-bearing rocks, and rocks displaying serpentine, sulfates of likely sedimentary origin..	**J. Mustard**, B. Ehlmann, J. Skok, D. Quinn, N. Mangold, D. Des Marais, S. Wiseman, J. Head, C. Edwards, R. Milliken, S. Parman, K. Cannon, T. Goudge, E. Amador, R. Harvey, M. Salvatore, M. Bramble, A. Brown, C. Viviano-Beck, F. Poulet, P. Niles, D. Rogers, T.	W1, W2, W3	1	3	selected among final 8	selected among final 3

						Glotch, S. Murchie, A. Fraeman, R. Hu, Y. Yung					
29	Jezero crater	18.4386	77.5031	-2.64	Delta stratigraphy, with access to olivine-rich carbonates, smectites, volcanics (crater floor).	**T. Goudge**, B. Ehlmann, C. Fassett, J. Head, J. Mustard, N. Mangold, S. Gupta, R. Milliken, W. Fischer, A. Brown, S. Karunatillake, J. Hurowitz, K. Kinch, S. Shahrzad	W1, W2, W3	4	1	selected among final 8	selected among final 3
30	Nili Fossae carbonate	21.7	78.8	-1.5	Phyllosilicates, carbonates, High-Mg mafic/ultramafic rocks emplaced in an uncertain setting.	**B. Ehlmann**, C. Edwards, J. Mustard, S. Wiseman, D. Rogers, T. Glotch, D. Archer, A. Fraeman, P. Niles, R. Hu, Y. Yung, C. Viviano-Beck, A. Brown	W1, W2	3	7	---	---
31	Hadriacus Palus	-26.919	77.971	-2.623	Rocks in a fluvio-lacustrine setting that include stratified units, paleo channels, and nearby igneous rocks..	**J. Skinner**, C. Fortezzo, T. Hare, K. Tanaka, T. Platz, C. Edwards, L. Edgar	W1, W2	16	21	---	---
32	Gale crater	-4.5	137.4	-4.5	Paleo lacustrine layered strata forming a record of a long-lived aqueous habitable environment in the Hesperian	**J. Grant**	W1	22	---	---	---
33	Columbia Hills (Gusev crater)	-14.55	175.45	-1.95	Rocks formed in a putative hydrothermal setting that incorporate opaline silica, phyllosilicates, carbonates, and sulfur-rich soil. Nearby Hesperian basalts.	**J. Rice**, S. Ruff, A. Longo, N. Cabrol, J. Farmer, E. Grin, J. Bishop, M. Salvatore, R. Arvidson, A. Zastrow, M. Wolff, M. Smith, J. Carter, D. Des Marais, C. Edwards, M. Kraft, P. Niles, K. Campbell, B. Damer, H. Nekvasil, D. Guido, M. Van Kranendonk, F. Westall, D. Lindsley, V. Hamilton, N. DiFrancesco, F. McCubbin	Pre-W1, W1, W2, W3	13	2	selected as final 8 site	selected among final 3
34	Eridania basin	-28.52	178.73	0.363	Sedimentary layers possibly emplaced in a paleolake deltaic/nearshore setting and that incorporate phyllosilicates and hydrated sulfates .	**M. Pajola**, S. Rossato, J. Carter, E. Baratti, M. Coradini, R. Pozzobon, M. Erculiani, K. McBride	W2	---	17	---	---

[a] Number corresponds to Figure 1. [b]Name given by presenter might not be an official USGS place name; [c]First person to present site is in bold but primary advocates may have changed throughout the selection process. [d]W1 (Workshop 1, May, 2014); W2 (Workshop 2, August, 2015); W3 (Workshop 3, February, 2017).

Figure 1.

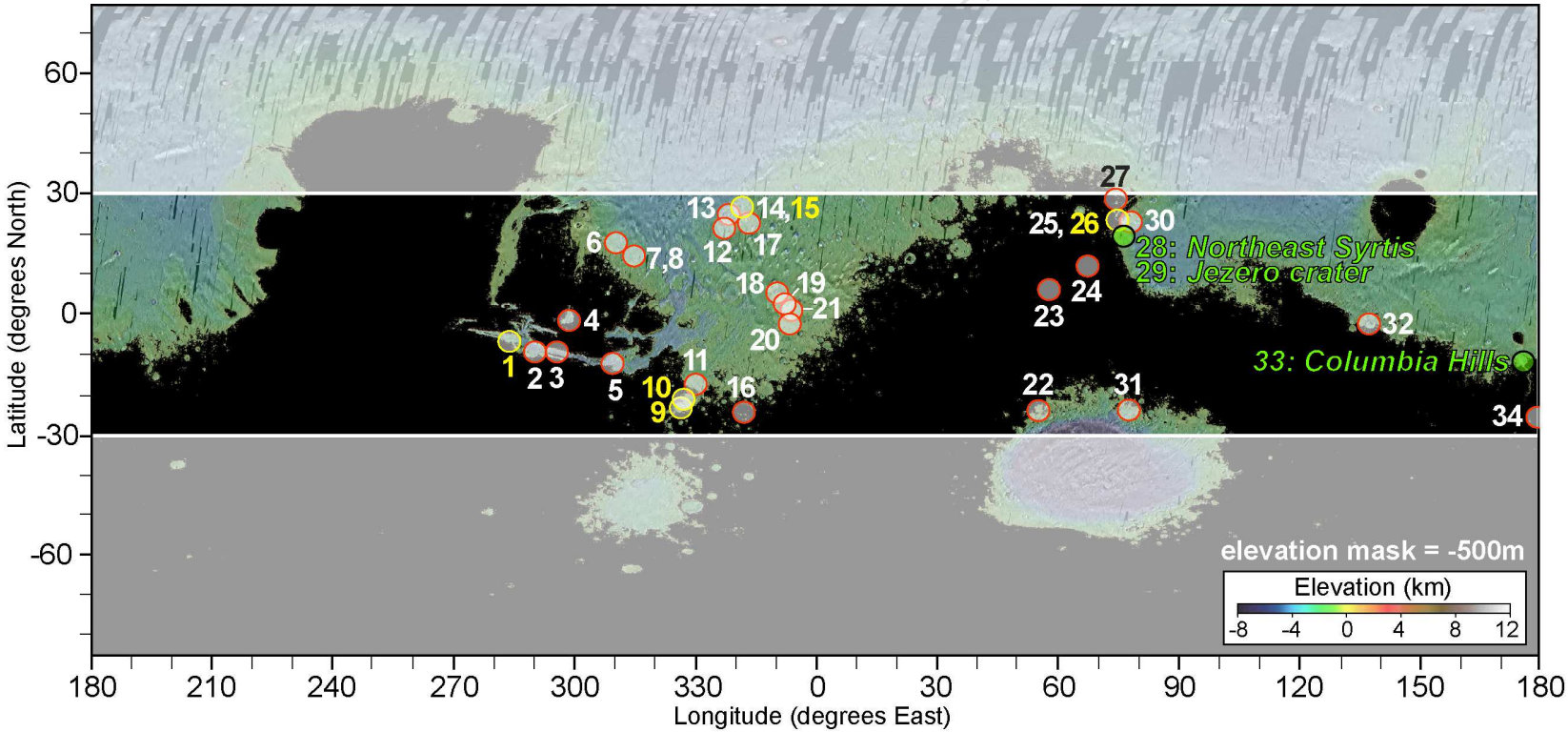
60
30
0
-30
-60
Latitude (degrees North)
180
210
240
270
300
330
0
30
60
90
120
150
180
Longitude (degrees East)
1
2 3
4
5
6
7,8
9
10
11
12
13
14,15
16
17
18
19
20
21
22
23
24
25, 26
27
28: Northeast Syrtis
29: Jezero crater
30
31
32
33: Columbia Hills
34
elevation mask = -500m
Elevation (km)
-8
-4
0
4
8
12

194 **Figure 1.** Global map of Mars (East longitude and degrees North latitude from ~75 to -90)
195 showing location all landing sites proposed for the Mars 2020 rover (See Table 6). Columbia
196 Hills (33), Jezero crater (29), Northeast Syrtis Major (28) in green represent the three final
197 candidate landing sites under consideration as of February, 2018. These three, plus the five sites
198 outlined in yellow round out the eight candidate sites remaining after the second workshop in
199 2015. Black and white shaded areas represent elevations (-500 m and above is black) and
200 latitudes (above 30°N and below 30°S is shaded white), respectively, which are outside the
201 safety and operation limits of the spacecraft (Table 3). Many of the sites proposed were in close
202 proximity to one another and the actual size of the landing ellipse is smaller than the dots
203 indicated on the map. Colorized MOLA data over global THEMIS daytime infrared data
204 (irregular black areas mostly above 60°N indicate gores in data coverage).
205
206 **3. The First Landing Site Workshop**
207 The first open science community landing site workshop for the Mars 2020 mission was held
208 near Washington, DC over three days in May, 2014. The workshop was attended by over 100
209 people, with an additional ~30 attending remotely each day (remote attendees did not participate
210 in the site evaluations). The workshop preceded selection of the instrument payload for the Mars
211 2020 Rover mission and attendees included many members of the Project and numerous
212 scientists unaffiliated with the mission at the time. A total of 27 candidate sites were presented
213 and discussed (Table 6, Figure 1), which included only 3 of the 9 pre-Workshop 1 sites (6 of the
214 pre-workshop sites were not presented at least in part due to analysis of pre-workshop imaging of
215 the sites that resulted in diminished interest). The 24 additional sites proposed (Table 6, Figure 1)

included a majority that had been forwarded as potential landing sites for previous rover missions such as MER and MSL.

There was a conscious effort to include presentations at the first workshop related to landing sites for the two MER rovers and the final four candidate sites for MSL whether or not there was advocacy from members of the science community. The rationale behind this decision was to provide insurance against loss of orbital assets used to collect data to characterize and certify landing sites. Because the ability to realistically evaluate the science potential and engineering risk of newly proposed sites would diminish significantly if orbital assets were lost, these potentially valuable sites from previous missions (albeit with differing science objectives) were considered because their surface characteristics were already known and could potentially be appropriate for the 2020 mission.

Three such sites not advocated by the community were Gale crater (MSL *Curiosity* landing site), Meridiani Planum (MER *Opportunity* landing site), and Holden crater (final candidate site for MSL). To ensure consistency and discussion of these potentially valuable prior sites, presentations were solicited by the co-chairs of the Mars Landing Site Steering Committee and the 2020 Project. The goal of these presentations was to assess and document whether the sites addressed Mars 2020 mission objectives and to determine if their lack of advocacy reflected a diminished need for additional characterization based on their prior consideration.

The objectives of the first workshop were to: 1) begin to evaluate which of the submitted sites were best suited to achieving science objectives of the 2020 Rover Mission within the constraints imposed by engineering requirements, planetary protection requirements, and the necessity of ensuring a safe landing; and 2) provide input to NASA and the 2020 Project on the relative importance of including any enhanced EDL capabilities on the mission. More

specifically, the workshop attendees voted to determine: 1) the site with the highest overall science merit; 2) sites that were most in need of additional imaging by orbital assets; 3) whether defined regions of interest (ROI) at the site were likely immediately accessible upon landing ("land on" site) or whether the ROIs were outside the landing ellipse and therefore required a traverse ("go to" site). The distinction is relevant for assessing the likely speed at which the mission can be successfully executed at each site. A ROI is an area identified from orbital data that best addresses the science objectives of the mission. Each ROI is a ~1 km area from which detailed study during the mission would lead to the collection of a number of rock and regolith samples. By contrast, a waypoint is an abbreviated campaign where only a single sample is acquired.

A major outcome of the workshop was a rank ordering of the proposed sites for use in future targeting for imaging by MRO and other orbital assets (Table 7). In addition, where possible, there was an initial discussion and assessment of how enhanced EDL capabilities such as Range Trigger and (or) Terrain Relative Navigation (TRN) (Golombek et al., 2015, 2016; Coombs, 2016; Farley and Williford, 2017) might improve the ability to land at a site or to improve access to a site (Table 7). Range Trigger specifies the latitude and longitude where the spacecraft parachute will open during EDL rather than using the spacecraft velocity, thereby shrinking the size of the landing ellipse by almost half (Coombs, 2016). TRN compares images taken during entry and descent with onboard orbital images of the surface in the ellipse, allowing the spacecraft to pinpoint its location with respect to surface features and to adjust its landing position to avoid hazardous terrain (Coombs, 2016).

It was clear from the discussion at the first workshop that the highest ranked candidate sites had a perceived science potential that could exceed the singular mission objectives for Mars

2020. The ability to cache samples with the possibility of eventual return to Earth clearly led workshop attendees to consider broader science questions related to Mars that might be addressed by future analyses of returned samples. Hence, candidate sites possessing a broad range of science ROIs encompassing a wide range of Martian history and relatable to important events in the Mars stratigraphic record ranked the highest (Table 7). Moreover, access to three of the top 10 sites likely required inclusion of Range Trigger during EDL and access to six of the top 10 sites definitely, probably, or might require TRN during EDL (Table 7). Recognizing the importance of including one or both of these enhanced EDL capabilities to enable landing at a range of high priority sites influenced the 2020 Project to continue studying their inclusion on the mission.

Of the three solicited presentations related to prior landing sites and landing site final candidate sites, only the Holden crater site ranked in the top third. The Gale crater and Meridiani Planum sites ranked in the bottom quartile and last, respectively (Table 7). Nevertheless, all of the sites proposed at the first workshop remained under consideration and were targeted for additional images (if requested by the proposer(s)) to better assess their science merit as well as engineering (Table 3) or planetary protection constraints (Table 1).

Following the first community workshop, the co-chairs of the Landing Site Steering Committee solicited all site proposers to provide additional imaging targets that were forwarded to the MRO science team for acquisition. These data were collected at the rate of ~3-5 targets per two-week long imaging cycle for nearly a year and required careful targeting based on input from site proposer(s) to maximize the ability to assess science characteristics. The ~140 total imaging targets submitted before and after the first workshop demonstrated an opportunity to target and quickly receive MRO images of study areas on Mars, which served as a powerful

incentive for the members of the science community to participate in the landing site selection process. More than 120 HiRISE images and approximately 35 CRISM images were acquired from the list of requests prior to the second landing site workshop.

Table 7. List of landing sites presented at the first workshop and voting assessment relative to various stated criteria (sorted by weighted average calculated using the sum of votes ranking a site high (3 points), medium (2 points) or low (1 point) divided by the number of votes for the site).

Landing Site	Weighted Average	Need for additional imaging	Is site a likely "land on (LO)" or "go to" (GT)?	Is Range Trigger likely needed for access?	Does Range Trigger reduce the need for TRN?	Does Access likely require TRN?	If "go to," would TRN likely make it a "land on?"
NE Syrtis	2.78	High	Mostly LO	Yes	Probably	Probably	No
Nili Fossae	2.59	Low	Mostly GT	No	Yes	Yes	No
Nili Fossae Carbonate	2.56	Low	LO	Yes	No	Yes	No
Jezero crater	2.33	Low	Partially GT	No	No	Yes	No
Holden crater	2.24	Low	GT	No	No	No	Probably
McLaughlin crater	2.24	Medium	Mostly LO	No	Probably	?	?
SW Melas Basin	2.22	Low	LO	Yes	No	Probably Not	No
Mawrth Vallis	2.16	Low	LO	No	No	No	No
East Margaritifer Chloride	2.13	Low	LO	No	No	Yes	No
Oyama crater	2.13	Medium	LO	No	No	No	No
Eberswalde crater	1.98	Low	GT	No	No	No	No
Ladon Valles	1.97	Medium	LO	No	No	No	Yes
Columbia Hills	1.91	Low	LO	No	No	No	No
Oxia Planum	1.80	High	LO	No	Probably	Probably	No
Nili Patera	1.84	Medium	Mostly GT	?	?	?	?
Hadriacus Palus	1.71	High	LO	No	Yes	Not with Range Trigger ellipse	No
Hypanis	1.65	Medium-High	LO and GT	No	Yes	?	?
Kashira crater	1.66	High	GT	Maybe	?	?	Probably
Circum-Hellas	1.55	Medium	GT	No	?	?	?
Coprates Chasma	1.52	Medium	Mostly GT	No	Probably	Probably	No
Sabrina Vallis	1.42	Medium	Partially GT	No	Yes	No	No
Gale crater	1.36	Low	GT	No	No	No	No
Firsoff crater	1.32	High	LO	No	No	No	No

Valles Marineris (Melas Chasma floor)	1.32	Medium	GT	No	?	?	?
Valles Marineris (Coprates Chasma)	1.28	Medium	GT	No	?	?	?
Valles Marineris (Juventae Chasma)	1.22	Medium	GT	No	?	?	?
Meridiani Planum	1.10	Low	LO	No	No	No	No

4. The Second Landing Site Workshop

The second open science community landing site workshop for the Mars 2020 mission was held in Arcadia, CA over 3 days in August, 2015. The second workshop was attended by ~150-190 participants from the science community and the Mars 2020 Project and instrument science teams, and an additional ~50 people participated each day remotely (remote attendees did not participate in the ranking of the sites).

The second workshop strongly focused on discussion of the science merits of the 21 candidate landing sites presented (Table 8). The candidate sites in Gale crater and Meridiani Planum were not presented at the workshop and did not receive further consideration. The goal of the workshop was to discuss the science merits of each site and provide a community ranking of the sites determined by voting on five scientific selection criteria. This input, in addition to other factors (e.g., engineering, operations, planetary protection), was assessed by the Mars 2020 Project to cull the list down to ~8 sites for continued consideration.

In order to guide discussion of the science merit of the sites towards topics the most relevant to the mission, a rubric was created by the Mars 2020 Project Landing Site Working Group (LSWG). The rubric was initially completed by workshop presenters in advance of the workshop and then updated in real time as sites were presented during the workshop: https://marsnext.jpl.nasa.gov/workshops/wkshp_2015_08.cfm. The rubric emphasizes Mars 2020 mission and science priorities defined in the Mars 2020 SDT report (Mustard et al., 2013) and the National Research Council decadal survey (NRC, 2011), and defines 24 landing site factors in four groups related to: 1) the environmental setting for biosignature preservation and taphonomy of organics; 2) the aqueous and geochemical environments indicated by mineral assemblages; 3) type of igneous samples present; and 4) context provided on sampled Martian

history and constraints on the timing of major events. The evolving entries in the rubric were viewable by both in-person and remote participants during the workshop and the updated and complete version was displayed on the last day prior to voting.

Five scientific selection criteria established by the Mars 2020 Project guided voting on the relative merits of the candidate sites. The criteria were derived from the mission science objectives and include: 1) confidence that the geologic setting and history of the landing site can be characterized and understood through a combination of orbital and in-situ observations; 2) evidence that the landing site offers an ancient habitable environment; 3) rocks with high biosignature preservation potential are available and accessible for investigation of astrobiological potential by the rover instrument suite; 4) the landing site offers an adequate abundance, diversity, and quality of samples suitable for addressing key astrobiological questions if and when they are returned to Earth; and 5) the landing site offers an adequate abundance, diversity, and quality of samples suitable for addressing key planetary evolution questions if and when they are returned to Earth (Table 8). These criteria were provided to presenters and attendees in advance of the workshop to help focus presentation content and discussion.

Following summary discussion on the final day of the workshop, workshop participants voted to rank the sites (Table 8). Voting involved assigning either a green (highest), yellow (intermediate), or red (lowest) color to each site. Voting order for the sites was determined by random drawing from a hat. Results of the voting (Table 8) were presented as both the mode (color receiving the most votes) and weighted average (where 5 points was given for each green vote, 3 for each yellow vote, and 1 for each red vote that was then summed and divided by the total number of votes). The weighted average ensured that participants could not skew the results

by withholding votes from some sites or by trying to favor a particular site by voting other sites red. Both methods yield similar results (Table 8) and reveal a fall-off in support for sites ranked lower than the top nine or ten based on mode and average, respectively. The rank ordering of the top ten sites in decreasing order based on weighted average was: Jezero crater (18.5°N, 77.4°E), Columbia Hills (Gusev crater, 14.4°S, 175.6°E), Northeast (NE) Syrtis Major (17.8°N, 77.1°E), Eberswalde crater (23.0°S, 327.0°E), Southwest (SW) Melas Basin (12.2°S, 290.0°E), Nili Fossae (21.0°N, 74.5°E), Nili Fossae Carbonate (21.9°N, 74.5°E), Mawrth Vallis (24.0°N, 341.1°E), Holden crater (26.4°S, 325.1°E), and McLaughlin crater (21.9°N, 337.8°E). These assessments from the workshop provided one form of community input into the science merits of the sites. This input was then weighed by the Mars 2020 Project and members of the Mars 2020 Landing Site Steering Committee immediately after the workshop against engineering, operations, and other factors to arrive at a final list of eight candidate sites remaining under consideration.

The one difference between the final eight candidate sites selected by the 2020 Project (Table 9) versus those identified by workshop rankings was the deletion of the 7th ranked Nili Fossae Carbonate site from consideration and the elevation of the 9th ranked Holden crater site into the final eight. McLaughlin crater was dropped because 2020 Project resources limited continued assessment to eight sites.

The rationale for removing the Nili Fossae Carbonate site from the final eight sites was based on a higher risk related to the engineering assessment and scientific overlap with other selected sites. Specifically, the ability to avoid landing in large fields of eolian bedforms (even with TRN) that appear inescapable (e.g., Golombek et al., 2012) at the Nili Fossae Carbonate site depended on a significant reduction in the landing ellipse that may not have been possible. Moreover, the

361 science and geological context proposed at the Nili Fossae Carbonate site is available at other
362 sites in the eight final candidate sites (e.g., NE Syrtis). Removal of the site from consideration
363 also allows focusing limited project resources on sites that are more likely to be acceptable from
364 a landing safety perspective.

365 **Table 8**. Assessment ranking of the candidate landing sites discussed and voted on by attendees at the second landing site workshop
366 relative to the five individual science criteria and overall average. Color of the cells correspond to the following scale: dark green (4.4-
367 5), light green (3.3-4.3), yellow (2.6-3.2), light red (1.5-2.5), dark red (1-1.4).
368

Rank	Site	Landing Site Scientific Selection Criteria										Overall Average	
		Characterizable Geologic Setting and History		Ancient Habitable Environment		High Biosignature Preservation Potential		Astrobiological quality of returned samples		Petrological quality of returned samples			
		Mode	Avg.	Mode	Avg.	Mode	Avg.	Mode	Avg.	Mode	Avg.	Mode	Avg.
1	Jezero crater	5	4.9	5	4.7	5	4.4	5	4.4	5	4.3	5	4.5
2	Columbia Hills	5	4.7	5	4.3	5	4.3	3	3.8	5	4.1	4.6	4.2
3	NE Syrtis	5	4.7	5	3.8	3	3.3	5	3.8	5	4.8	4.6	4.1
4	Eberswalde crater	5	5.0	5	4.5	5	4.3	3	3.4	3	3.0	4.2	4.0
5	SW Melas	5	4.5	5	4.1	5	3.9	3	3.6	3	3.1	4.2	3.9
6	Nili Fossae	5	4.4	3	3.4	3	3.2	3	3.4	5	4.7	3.8	3.8
7	Nili Fossae Carbonate	5	4.2	3	3.4	3	3.2	3	3.2	5	4.3	3.8	3.7
8	Mawrth Vallis	5	4.3	3	3.7	3	2.9	3	3.4	5	3.9	3.8	3.6
9	Holden crater	5	4.4	3	3.4	3	3.2	3	3.2	3	3.4	3.4	3.5
10	McLaughlin crater	3	3.6	3	3.9	3	3.0	3	3.5	3	3.5	3	3.5
11	Hypanis	3	3.8	3	3.6	3	3.1	3	3.0	3	2.8	3	3.2
12	Nili Fossae South	3	3.8	3	2.9	3	2.6	3	2.9	3	3.9	3	3.2
13	Ladon Valles	3	3.8	3	3.3	3	3.1	3	2.7	3	2.7	3	3.1
14	E. Margaritifer	3	3.7	3	3.1	3	3.5	3	2.7	3	2.7	3	3.1
15	Coprates Chasma	5	4.1	3	2.7	3	2.3	3	2.5	3	3.7	3.4	3.1
16	Oyama crater	3	3.3	3	3.2	3	2.8	3	2.7	3	3.1	3	3.0
17	Eridania	3	3.2	3	2.8	3	2.5	3	2.3	3	2.4	3	2.6
18	Nili Patera	5	4.6	3	2.4	3	2.5	1	1.4	3	2.2	3	2.6
19	Oxia Planum	3	3.0	3	2.4	1	2.1	1	2.1	3	2.7	2.2	2.5
20	Sabrina/Magong crater	3	3.1	3	3.0	3	2.2	1	1.8	1	2.0	2.2	2.4
21	Hadriacus Palus	3	3.2	3	2.5	1	1.5	1	1.6	3	2.8	2.2	2.3

Table 9. Details of the proposed landing ellipse for the final eight candidate sites for the Mars 2020 Mission (listed alphabetically). Location of ellipse center point, elevation and size with the long axis oriented approximately east-west.

Landing Site	Latitude (°N)	Longitude (°E)	Approximate Elevation (km)	Approximate Buffered Ellipse Axes (km)
Columbia Hills	-14.5478	175.6255	-1.93	9.6 x 8.7
Eberswalde crater	-23.7749	-33.5147	-1.49	8.6 x 7.7
Holden crater	-26.6130	-34.8167	-2.18	9.5 x 8.1
Jezero crater	18.4386	77.5031	-2.64	10.7 x 8.3
Mawrth Vallis	23.9685	-19.0609	-2.24	11.9 x 9.8
NE Syrtis	17.8899	77.1599	-2.04	11.1 x 8.2
Nili Fossae	21.0297	74.3494	-0.65	9.7 x 7.7
SW Melas Basin	-9.8132	-76.4679	-1.92	9.7 x 8.7

5. Overview of the Final Eight Candidate Landing Sites

5.1 Introduction to Final Eight Sites

The final eight Mars 2020 sites (Figure 2), with the exception of Columbia Hills, were prior candidates for the MSL landing site, and three (Eberswalde crater, Holden crater, and Mawrth Vallis) were among the final four MSL candidate sites. A summary of the perceived science potential and interpretations after the second workshop and up to the third workshop is presented (Figure 2), though it is important to note that collection of additional data and interpretations made since that time resulted in some evolution in the interpretations of setting and (or) merit of some of the sites.

Three of the final eight sites target locales where exposed rocks may reveal evidence of biosignatures in ancient habitable environments in the subsurface (Nili Fossae, NE Syrtis, and Mawrth Vallis). Half of the top-ranked landing sites are deltaic or lacustrine environments (Eberswalde crater, Holden crater, Jezero crater, SW Melas Basin) reflecting the strong belief within the science community that rocks in deltaic settings are favorable for the preservation of biosignatures of ancient life if it ever developed on Mars (Summons et al., 2010). The Columbia

Hills site provides access to rocks emplaced in a putative hot spring setting and is likely representative of a unique, potentially astrobiologically relevant environment relative to those accessible at the other sites. Preliminary engineering analyses of the final eight sites show that Terrain Relative Navigation (TRN) is required to ensure access to most. Only one was viewed as a certain non-TRN site (Nili Fossae), while two others (Columbia Hills and Holden crater) may or not may be safely accessible without TRN. A brief summary of the final eight candidate sites based on previously published work follows, in the order of broad geological setting as described above.

5.2 Ancient Subsurface Environments

Three of the eight final sights, Nili Fossae and NE Syrtis, located northwest of the Isidis basin, and Mawrth Vallis further to the west, are locations that may record ancient subsurface habitable environments, possibly related to past groundwater circulation (e.g., Michalski et al., 2013; 2017). These sites may also be analogous to ancient subsurface/lithospheric environments harboring microbial ecosystems on the Earth (Sherwood Lollar et al., 2014).

5.2.1 Nili Fossae: Hargraves Ejecta, Trough Clays, Lavas, and Ancient Altered Rocks

At Nili Fossae, a sequence of geologic events was defined that lead to the definition of scientific ROIs that are “land on” on the floor of the trough and “go to” within a trough reentrant or valley west of the candidate ellipse that exposes regionally occurring Noachian-aged materials (Figure 2A). Both would sample potential subsurface crustal refugia protected from harsh surface conditions (e.g., exposure to radiation, see Mustard and Tarnas, 2017) through the Noachian and orbital data indicate the presence of altered and unaltered materials. The proposed landing ellipse is located on the floor of the trough that is partially covered by unaltered Hesperian-aged lava flows (Hiesinger and Head, 2004). The lava flows are underlain by clay-

411 bearing rocks exposed on the west side of the trough and are overlain by impact ejecta from the
412 Hargraves crater to the east. Orbital data does not define the depositional setting associated with
413 the clay-bearing material on the floor of the trough, though it is presumed to be sedimentary in
414 origin (Ehlmann et al., 2009). The Hargraves ejecta includes blocks of unaltered crustal
415 materials, carbonate-bearing materials (Ehlmann et al., 2008b), clay-bearing materials either
416 excavated by the impact or formed by *in situ* alteration in post-impact hydrothermal systems, and
417 could also include impact glasses (Ryan et al., 2017) (Figure 2B). A proposed sampling
418 waypoint between the Hargraves ejecta ROI and the trough reentrant, or valley to the west,
419 would access Hesperian lava flows from Syrtis Major and the underlying clay-bearing rocks. The
420 reentrant itself would provide access to altered rocks that include carbonates, serpentine, and
421 aluminum-clay-bearing rocks of unknown origin, and unaltered low calcium pyroxene Noachian
422 crustal materials (Mustard et al., 2008, 2010; Poulet et al., 2005) (Figure 2C). The diversity of
423 accessible rocks and alteration products may indicate that they formed in a variety of subsurface
424 and (or) surface environments including hydrothermal (e.g., Osinski et al., 2012), alluvial/fluvial,
425 and shallow crust/pedogenic settings that were potentially habitable (Mangold et al., 2007;
426 Ehlmann et al., 2010; Mustard et al., 2008, 2010; Michalski et al., 2010; Michalski et al., 2017).

427 *5.2.2 NE Syrtis: Ancient Stratigraphy of Altered Rocks with Clays and Carbonates*

428 The proposed landing site in NE Syrtis is primarily a “land on” site located south of the Nili
429 Fossae site just north of the Syrtis Major volcanics (Figure 2D). The candidate site possesses
430 distinct, diverse units exposing Hesperian and Noachian-aged sequences with hydrated and
431 phyllosilicate mineral signatures (Bibring et al., 2005, 2006; Poulet et al., 2007; Mustard et al.,
432 2008, 2010; Ehlmann et al., 2010) (Figure 2E) whose origin is sandwiched between materials
433 associated with the ~3.8-3.9 Ga (Frey, 2008) Isidis basin impact and the later emplacement of

Hesperian Syrtis Major lavas. More specifically, the surface is incised by a number of channel networks, contains local basins, and is characterized by a series of mesas and intervening valleys within the ellipse. This topography provides outcrops that expose diverse stratigraphy at the decameter scale, ranging in age from the Early Noachian to the Hesperian (Ehlmann and Mustard, 2012; Bramble et al., 2017).

Mesa stratigraphy includes clay-bearing basement rocks that are overlain by a carbonate-bearing olivine-rich unit that is all capped by a mafic, crater-retaining cap that may be related to Syrtis Major lavas (Mangold et al., 2007; Ehlmann and Mustard, 2012) (Figure 2F). The basement is characterized by megabreccia blocks within a more massive, iron and magnesium clay-bearing unit and local occurrences of a kaolin-group mineral and an Al-phyllosilicate weathering horizon (Bramble et al., 2017). By contrast, the overlying and regionally extensive olivine-rich unit displays some megabreccia blocks and is variably fractured and altered to contain up to ~20% carbonate, hypothesized to represent ancient shallow mineralization of the host rock or perhaps precipitation in mineral springs (Ehlmann and Mustard, 2012; Bramble et al., 2017; Salvatore et al., 2018). Either or both of the sections comprising the basement rocks and olivine-rich carbonate-bearing rocks could be of volcanic and (or) impact origin that has been modified by later groundwater processes (Bramble et al., 2017). Any of the numerous locations where this stratigraphy is accessible in the ellipse form possible ROIs, with a number of distributed locations identified that provide access to the Noachian clay-bearing basement, carbonates and basalt cap. Finally, Hesperian-aged sulfates and overlying Syrtis Major volcanic rocks occur outside of the ellipse to the south and represent potential extended mission exploration targets (Ehlmann and Mustard, 2012; Quinn and Ehlmann, 2018). The diversity of rocks exposed at NE Syrtis records a transition from neutral to alkaline pH and can be related to

457 up to four distinct aqueous environments that occurred in the region (Bramble et al., 2017). The
458 associated observed mineral signatures may support evidence for the evolution of past habitable
459 environments (Farmer and Des Marais, 1999) that could be interrogated by the Mars 2020 rover.

460 *5.2.3 Mawrth Vallis: Widespread Ancient Noachian Stratigraphy with Abundant Clay*

461 The Mawrth Vallis candidate landing site is located on a plateau in the upland region
462 between Mawrth Vallis and Oyama crater in northwestern Arabia Terra (Figure 2G). The
463 Mawrth site is "land on" and is characterized by a thick (>60 m), widespread, and layered
464 sequence of diverse and abundant phyllosilicates and other aqueous phases, such as Si-OH
465 phases and sulfates, that can be broadly divided into three units: a regional plateau unit; an inter-
466 crater plateau unit, and the Oyama crater floor deposits (Loizeau et al., 2012, 2015). All three
467 units were likely formed in order from the Early through the Late Noachian during an extended
468 phase of aqueous alteration very early in Mars' history and were later capped by a relatively
469 darker-toned unit in the Early to Late Hesperian that may be volcanic/pyroclastic in origin
470 (Loizeau et al., 2012, 2015).

471 Exposed rocks are incised by multiple valley network systems, incorporate phyllosilicates
472 and likely reflect a complex aqueous history and alteration of basalt (Bibring et al., 2005; Poulet
473 et al., 2005; Loizeau et al., 2007; Michalski and Noe Dobrea, 2007; Bishop et al., 2008; Wray et
474 al., 2008). Within the Mawrth sequence and the ellipse, clays dominate with Al-phyllosilicates
475 and hydrated silica separated from underlying Fe/Mg phyllosilicates without any observable
476 inter-bedding and by a ferrous horizon that forms a likely unconformity (Figures 2H, 2I). Upper
477 portions of the lower Fe/Mg phyllosilicate unit display mineralized fractures and there are also
478 local occurrences of sulfate deposits (basanite, jarosite, alunite) in the upper Al-phyllosilicate
479 and hydrated silica unit (Loizeau et al., 2012). However, other mineralogies are also present and

include ferrihydrite, allophane (near the top of the sequence), kaolinite, and others (Loizeau et al., 2012). Proposed ROIs include numerous locations that provide access to multiple clay units, mineralized fractures, and the dark cap rock and all occur within the candidate ellipse.

While at least some of the layered materials predate incision of nearby Mawrth Vallis (Loizeau et al., 2010), it is unclear when their alteration ended, as development of the uppermost Al-phyllosilicate bearing units may post-date formation of Mawrth Vallis (Wray et al., 2008). The phyllosilicates also outcrop well to the south of Mawrth Vallis (Noe Dobrea et al., 2010), and such a broad extent could imply they formed *in situ*. Although the Mawrth layered materials may reflect pedogenic alteration (Loizeau, 2010) or aqueous alteration of volcanic ash deposits (Noe Dobrea et al., 2010), the depositional setting remains uncertain (Bibring et al., 2005; Michalski and Noe Dobrea, 2007; Bishop et al., 2008; Wray et al., 2008; Noe Dobrea et al., 2010). Nevertheless, it is clear from the detected mineralogy that a number of aqueous alteration and potentially habitable environments were present over an extended period at the Mawrth site (Loizeau et al., 2015), and the collective properties of the site suggest that preserved biosignatures may be present (Bishop, 2017). Moreover, the diversity of rocks associated with all of the major units should be readily accessible to the Mars 2020 rover and ongoing eolian erosion indicates an abundance of relatively recently exposed outcrops (Loizeau et al., 2015).

5.3 Deltaic or Lacustrine Environments

Four of the final eight candidate sites represent ancient deltaic or lacustrine environments, of interest because they reflect deposition in a low energy, long-lived lacustrine setting. On Earth, lacustrine facies have predictable properties that can include deposition/formation of fine-grained clays and, they are associated with the concentration and burial of organics and biosignatures

(Farmer and Des Marais, 1999; Summons et al., 2010). These four sites are Eberswalde crater, Holden crater, Jezero crater, and southwest Melas basin.

Two of the candidate deltaic sites are within Holden and Eberswalde craters, both located in the ancient cratered terrain of southern Margaritifer Terra (Scott and Tanaka, 1986). Eberswalde crater is likely Late Noachian in age (Moore et al., 2003; Pondrelli et al., 2005, 2008; Rice et al., 2013; Irwin et al., 2013, 2015), whereas Holden crater formed in the Hesperian (Grant et al., 2008; Mangold et al., 2012; Rice et al., 2013; Irwin and Grant, 2013; Irwin et al., 2013, 2015). Both craters excavated deposits filling the Early Noachian Holden basin (Saunders, 1979; Schultz et al., 1982; Frey et al., 2003) and contain distinctive stratigraphic and morphologic expressions of deltaic/lacustrine sedimentation that were deposited no earlier than the Hesperian (Moore et al., 2003; Mangold et al., 2012; Rice et al., 2011, 2013; Irwin et al. 2013). These deposits also coincide with phyllosilicate mineral enrichments (Grant et al, 2008; Milliken and Bish, 2010), which points to accumulation in a body of standing water.

5.3.1 Eberswalde Crater: The Best Preserved Delta on Mars

Eberswalde crater predates and lies just to the north of Holden crater and ejecta from Holden (including some large blocks of megabreccia containing multiple fragments and (or) lithologies) partially mantle the floor of Eberswalde and modified its southern rim (Rice et al., 2013) (Figure 2J). A period of faulting, perhaps accompanied by hydrothermal activity that filled some fractures, was followed by wall incision and formation of a closed-basin lake in which at least six distinct fluvio-deltaic systems formed (Rice et al., 2011, 2013). By far the largest of these is a broad fluvial delta that occurs along the western wall of Eberswalde crater (Malin and Edgett, 2003; Moore et al., 2003; Lewis and Aharonson, 2006), and was likely deposited over a period ranging from decades (Jerolmack et al., 2004) to more than a hundred thousand years

(Bhattacharya et al., 2005) or even a million years (Irwin et al., 2013). Detailed study of channel and delta morphometry suggest formation is consistent with either intermittent rainfall of ~1 cm/day or snowmelt (Irwin et al., 2013). The delta, incorporating phyllosilicates, likely eroded from the source basin to the west of the crater (Mangold et al., 2012), built into a lake covering a portion of the crater floor (Pondrelli et al., 2008; Milliken and Bish, 2010; Mangold et al., 2012; Irwin et al., 2013). Though modified by subsequent mantling/erosion (Rice et al., 2013) much of the primary morphology associated with the fan delta is preserved and would be accessible to the Mars 2020 rover (including possible bottomset beds).

The candidate landing ellipse (Figure 2J) encompasses the distal eastern portion of the large western fan deposit as well as a portion of the crater floor farther to the east. Multiple ROIs along the distal, eastern margin of the delta can be placed somewhat west to southwest of the center of the ellipse, thereby enabling “land on” exploration at Eberswalde. ROIs provide access to a set of high priority exploration targets that includes possible delta bottomset and lacustrine deposits as well as possible delta foreset beds (Figure 2K), outcrops of Holden crater ejecta or megabreccia, and large vein-filled fractures (Figure 2L) (e.g., see Rice et al., 2011, 2013 for description of units). Examples of potential extended mission ROIs occur in nearly all directions from the ellipse and include the top of the western fan delta, younger delta lobes/deltas to the south, and basement rocks east of the ellipse.

5.3.2 Holden Crater: Alluvial Fans, Putative Lacustrine Deposits, and Megabreccia

The candidate landing site in the southwest corner of Holden crater (Figure 2M) is located on a broad alluvial bajada flanking portions of the western wall of the crater (Moore and Howard, 2005; Pondrelli et al., 2005; Grant et al., 2008). The crater wall and rim sourcing the fans expose numerous blocks of impact megabreccia that are sometimes bedded and up to 50 m across

548 (Figure 2O) and likely excavated from sedimentary fill in Holden basin during crater formation
549 (Grant et al., 2008, 2010). The fans forming the bajada onlap relatively lighter-toned and finely-
550 layered rocks to the east that cover much of the crater floor (Malin and Edgett, 2000; Pondrelli et
551 al., 2005; Grant et al., 2008). Clay abundance decreases (Milliken et al., 2008; Milliken and
552 Bish, 2010) and the expression of bedding increases up section (Grant et al., 2008, 2010b). The
553 finely layered rocks were locally eroded and variably mantled by deposits associated with an
554 elongate fan delta deposit emanating from a wall breach associated with Uzboi Vallis to the
555 south (Grant et al., 2008, 2010, 2011). These deposits are interpreted to have formed by two
556 distinct lakes of differing character and sources during the Hesperian (Grant el al., 2008, 2010;
557 Irwin et al., 2013). The first lake was likely relatively long-lived and sourced by drainage from
558 the wall-flanking fans and may include distal alluvial deposits. By contrast, the second lake was
559 shorter-lived and created when water impounded in Uzboi Vallis breached Holden's rim and
560 rapidly drained into the crater (Grant et al., 2011). Late runoff from the fans may have been fed
561 by snowmelt occurring in source alcoves along the crater rim (Grant and Wilson, 2012).

562 Holden crater ROIs are outside of the landing ellipse and include "go to" access to a
563 complete section of the finely layered likely lacustrine and distal alluvial beds and impact
564 megabreccia blocks as the highest priority (Figures 2N, 2O). "Land on" interrogation of alluvial
565 fan deposits within the ellipse is a somewhat lower priority. The candidate ellipse is located on
566 the variably deflated fan surface (as evidenced by inverted distributary channels) to minimize
567 landing hazards. The fan surface is partially covered in some locations by mostly NW-SE
568 trending eolian bedforms (Grant et al., 2008, 2010) that could impede rover trafficability and
569 delay arrival at the prime ROIs. Potential extended mission ROIs include additional outcrops of

570 the likely lacustrine beds and the younger fan delta deposits associated with flooding from
571 discharge out of Uzboi Vallis.

572 *5.3.3 Jezero Crater: A Well-Exposed Noachian Delta with Clays and Carbonates*

573 Jezero crater, northeast of the NE Syrtis site and south of Nili Fossae, is the site of an open-
574 basin paleolake that was ~250 m deep and sourced by two valleys with well-preserved deltas at
575 their mouths that flank the west and northwest crater wall (Fassett and Head, 2005, 2008a;
576 Ehlmann et al., 2008a; Goudge et al., 2012, 2015, 2017a, 2017b) (Figure 2P). The distinctive
577 stratigraphic and morphologic expressions of deltaic/lacustrine sedimentation coincide with
578 phyllosilicate mineral enrichments (Ehlmann et al., 2008a) (Figure 2Q). The lake was drained by
579 an eastern outlet (Fassett and Head, 2005, 2008a) during the Late Noachian, and fluvio-deltaic-
580 lacustrine activity ceased near the time of the Noachian-Hesperian boundary (Fassett and Head,
581 2008b). The associated drainage basins for the deltas extended well to the west and north of the
582 crater and cover and sampled (via transport) diverse materials that may have included those
583 associated with the ejecta at Hargraves crater (Fassett and Head, 2005; Ehlmann et al., 2008a;
584 Goudge et al., 2017a). Delta deposits are underlain by Mg-carbonate basin fill that may be
585 detrital (Ehlmann et al., 2009; Schon et al., 2012) or part of a more regional deposit (Goudge et
586 al., 2015) (Figure 2R). A capping unit that may or may not be volcanic embays both deltas,
587 covers most of the present-day floor of the crater, and was likely emplaced during the Late
588 Hesperian or Early Amazonian (Schon et al. 2012; Goudge et al., 2015).

589 The candidate landing ellipse (Figure 2P) is located inside the crater on the capping unit that
590 mostly covers the crater floor and is mostly east of phyllosilicate-bearing, late-Noachian delta
591 deposits extending from the west and northwest walls (Fassett and Head, 2005; Ehlmann et al.,
592 2008a). ROIs are generally located in the western part of the ellipse, with proposed successive

593 "land on" interrogation of the floor deposits, carbonate basin fill (Figure 2R), and the clay-
594 bearing distal edge of the southern delta where bottomset and lacustrine beds with possible
595 concentrations of organics or biosignatures could be accessible (Figure 2Q). Additional possible
596 ROIs include likely erosional remnants to the east of the main delta as well as foreset beds in the
597 delta. Extended mission "go to" ROIs include ancient channel deposits on the top of the delta or
598 even longer-term access to the Jezero crater wall and beyond to the west.

599 *5.3.4 Southwest Melas Basin: Delta and Lacustrine Deposits in Valles Marineris*

600 The candidate landing site in SW Melas Basin (Figure 2S) is the location of a paleolake
601 formed within a ~30 km-long basin perched on the southern wall of the larger Melas Chasma in
602 Valles Marineris (Quantin et al., 2005; Dromart et al., 2007; Metz et al., 2009; Williams and
603 Weitz, 2014; Weitz et al., 2015; Edgar and Skinner, 2016; Davis et al., 2017). The basin is more
604 than 4 km below the plains bounding the canyon and is more than 1 km above the canyon floor
605 (Quantin et al., 2005). Two sub-basins within the broader basin preserve a variety of layered
606 sedimentary units that were sourced from multiple igneous and draping sedimentary
607 materials/rocks in the wall above and from basaltic and sedimentary units on the plains bounding
608 the edge of the canyon (Mangold et al., 2004; Williams and Weitz, 2014; Weitz et al., 2015;
609 Davis et al., 2017). At least two tributary systems drain directly to the lake, although additional
610 drainages bypass to the floor of the chasma and indicate more widespread runoff occurred when
611 the lake was present (Davis et al., 2017). Up to 11 individual fans positioned above and below a
612 marker bed (Williams et al., 2014) record multiple lakes (two main phases) that rose to varying
613 levels in the basin (Mangold et al., 2004; Williams et al., 2014; Weitz et al., 2015; Davis et al.,
614 2017) and persisted over periods of at least hundreds (Williams et al., 2014) to perhaps

615 thousands of years (Metz et al., 2009) or even longer (Irwin et al., 2015) during the Hesperian
616 (Williams et al., 2014; Weitz et al., 2015; Davis et al., 2017).

617 Individual basin units include convoluted bedded, planar bedded, clinoform (sloping
618 depositional surfaces often occurring in a delta front), and fan deposits (Edgar and Skinner,
619 2017) (Figure 2T). Some deposits incorporate opal and jarosite (Figure 2U) that is consistent
620 with deposition occurring fairly late in Martian history (Williams et al., 2014; Weitz et al., 2015).
621 At least some of the beds associated with these units were likely deposited in sublacustrine fans
622 (Metz et al., 2009) and some within one sub-basin are convoluted (Edgar and Skinner, 2017),
623 perhaps deformed by subaqueous landslides or liquefaction (Metz et al., 2010). Careful mapping
624 reveals the presence of a marker bed that helps to distinguish lake episodes (Williams and Weitz,
625 2014). Finally, a layered drape of likely airfall materials >100 m thick buried and then was
626 partially eroded to re-expose the lacustrine beds (Weitz et al., 2015; Davis et al., 2017),
627 suggesting that any organics and (or) biosignatures that may have been concentrated in the fans
628 and lacustrine deposits could have been largely shielded from irradiation and remain preserved in
629 beds that were geologically recently exposed.

630 The landing ellipse is placed to provide “land-on” access to deltaic deposits and multiple
631 lacustrine deposits emplaced at differing times and at differing depths (e.g., Metz et al., 2009,
632 Williams et al., 2014). Two specific types of ROIs are located in multiple locations to provide
633 access to deep subaqueous fan deposits (Metz et al., 2009) (Figure 2T) and younger opal-bearing
634 deposits (Williams and Weitz, 2014; Weitz et al., 2015) (Figure 2U) regardless of where the
635 rover was to touch down in the ellipse. The deep subaqueous fan deposits are likely characterized
636 by fine-grained sediments that may preserve organics and (or) biosignatures if they existed,
637 whereas the opal-bearing deposits are associated with isolated, relatively lighter-toned outcrops

638 that could be related to either past hydrothermal, diagenetic, or primary precipitate processes, or
639 even subsequent mineral replacement. Potential extended mission "go to" targets include the
640 clinoform unit and associated sulfates (Dromart et al., 2007) or access to rocks enabling study of
641 the broader sedimentary and tectonic processes that have shaped Valles Marineris over time.

642 5.4 Columbia Hills: Putative Hot Spring Silica and Lacustrine Carbonate Deposits

643 The Columbia Hills site (Figure 2V) is within Gusev crater which lies at the downstream
644 terminus of Ma'adim Vallis. The floor of Gusev may have hosted lacustrine sediments, deposited
645 by water draining from Ma'adim Vallis (Cabrol et al., 1996, 2001; Cabrol and Grin 1999; Irwin
646 et al., 2002), but they are now largely buried by Hesperian-aged basalts (Milam et al., 2003;
647 Greeley et al., 2004; McSween et al., 2004; Golombek et al., 2006). The ROIs identified for the
648 landing site are "land on" and largely centered on hills embayed by the volcanic plains materials
649 informally named "Columbia Hills." Possible outcrops of unknown, but possible lacustrine and
650 (or) deltaic materials occur outside the ellipse to the south (e.g., Cabrol et al., 1996; 2001; Cabrol
651 and Grin, 1999).

652 The Columbia Hills were first suggested as a future sample return landing site based upon the
653 field investigations and discoveries made by the *Spirit* Mars Exploration Rover (Rice, 2010).
654 Portions of the candidate landing site that include the primary ROIs were explored by the *Spirit*
655 Rover between 2004 and 2010 (e.g., Squyres et al., 2004, 2007, 2008), thereby enabling
656 assessment for the Mars 2020 mission to draw upon data collected *in situ* at scales many times
657 higher relative to the resolution of orbital data available for all other sites. The *Spirit* rover
658 landed on and initially traversed impact and eolian modified volcanic plains (e.g., Grant et al.,
659 2006a; 2006b; Golombek et al., 2006). *Spirit* later found abundant evidence of aqueous activity
660 and alteration of soils and rocks in the Columbia Hills (Squyres et al., 2006) (Figure 2W) and

661 volcaniclastic sediments around an eroded volcanic edifice dubbed “Home Plate” (Squyres et al.,
662 2007; Lewis et al., 2008). Materials discovered include carbonates at an outcrop informally
663 named “Comanche” (Ruff et al., 2014) and opaline silica (Squyres et al., 2008; Ruff et al., 2011)
664 (Figure 2X) near the end of the rover traverse. The opaline silica may be related to past fumarolic
665 acid-sulfate leaching or precipitation at steam vents or hot springs (Squyres et al., 2008; Ruff et
666 al., 2011) and occurs in a variety of forms that includes outcrops characterized by centimeter to
667 decimeter-scaled nodular and digitate features (e.g., Ruff et al., 2011; Ruff and Farmer, 2016)
668 (Figure 2X) that may be analogous to similar appearing features observed in terrestrial hot spring
669 deposits in Chile (Ruff and Farmer, 2016; Ruff et al., 2018). Because formation of digitate
670 features at terrestrial hot spring deposits can include contributions from microbes, the possibility
671 of similar microbial contributions to the digitate forms on Mars is of special interest. However,
672 there is a lack of consensus regarding whether the Martian forms are the result of outcrop erosion
673 on a scale similar to that thought to be responsible for shaping the surrounding landscape (e.g.,
674 Arvidson et al., 2008; McCoy et al., 2008; Ruff et al., 2018), or if they are primary depositional
675 forms (e.g., Ruff et al., 2018). Uncertainty also remains regarding whether sample handing
676 capabilities on the 2020 rover can acquire and collect the digitate features (Figure 2X).
677 Nevertheless, the outcrops expressing digitate features that may represent primary depositional
678 forms associated with past biological activity are the reason they are proposed as the primary
679 target for exploration by the 2020 rover at the Columbia Hills site. Secondary and possible
680 extended mission exploration targets include the Comanche carbonates and sampling the
681 Hesperian-aged lava plains around the Hills and within the ellipse and the possible
682 lacustrine/deltaic deposits outside the ellipse to the south, respectively.

683 5.5 Continued Characterization and Further Analyses of the Final Eight Sites

684 Continued collection of orbital data for all eight remaining candidate sites after the second
685 workshop was overseen by the co-chairs of the Landing Site Steering Committee and enabled
686 further evaluation of the engineering and science merits of each. Additional imaging also enabled
687 production of digital elevation models (DEMs), rock maps, and other special products to refine
688 landing and traverse hazards, produce mature estimates of traverse distance and time to various
689 ROIs, and enable further evaluation of science potential and risk. To assist in site evaluation, site
690 proposers from the science community were engaged to identify, refine, and prioritize a more
691 mature set of ROIs and waypoints within each site that best address the science objectives of the
692 mission based on the suite of data in hand and would lead to the collection of 16 samples and 4
693 blanks during the nominal mission.

694 The 2020 Project evaluated the distance and time required to visit each ROI and waypoint for
695 each landing site. The traverse time was evaluated using criteria that impact rover mobility and
696 included: study of the surface slopes over 1 m length-scales; the derived rock abundance; and
697 terrain maps showing the extent and orientation of eolian ripples and other potential impediments
698 to mobility. The time taken to reach the ROIs was based on an estimated driving efficiency of
699 35-75 m/sol and avoidance of areas in the ellipse that could not be accessed by the rover. For
700 each landing point in the ellipse, the minimum distance and drive time needed to visit the
701 proposed science ROIs and waypoints were determined.

702 The goal of the work done after the second workshop and prior to the third workshop was to
703 acquire the best and most complete data set possible for comprehensive discussion of the final
704 eight sites at the third community landing site workshop. Collectively, 193 HiRISE and nearly 70
705 CRISM images were acquired of these candidate landing sites by the time of the third Mars 2020

706 landing site workshop and included the completion of almost all of the requested targets at that
707 time.

708 **Figure 2.**

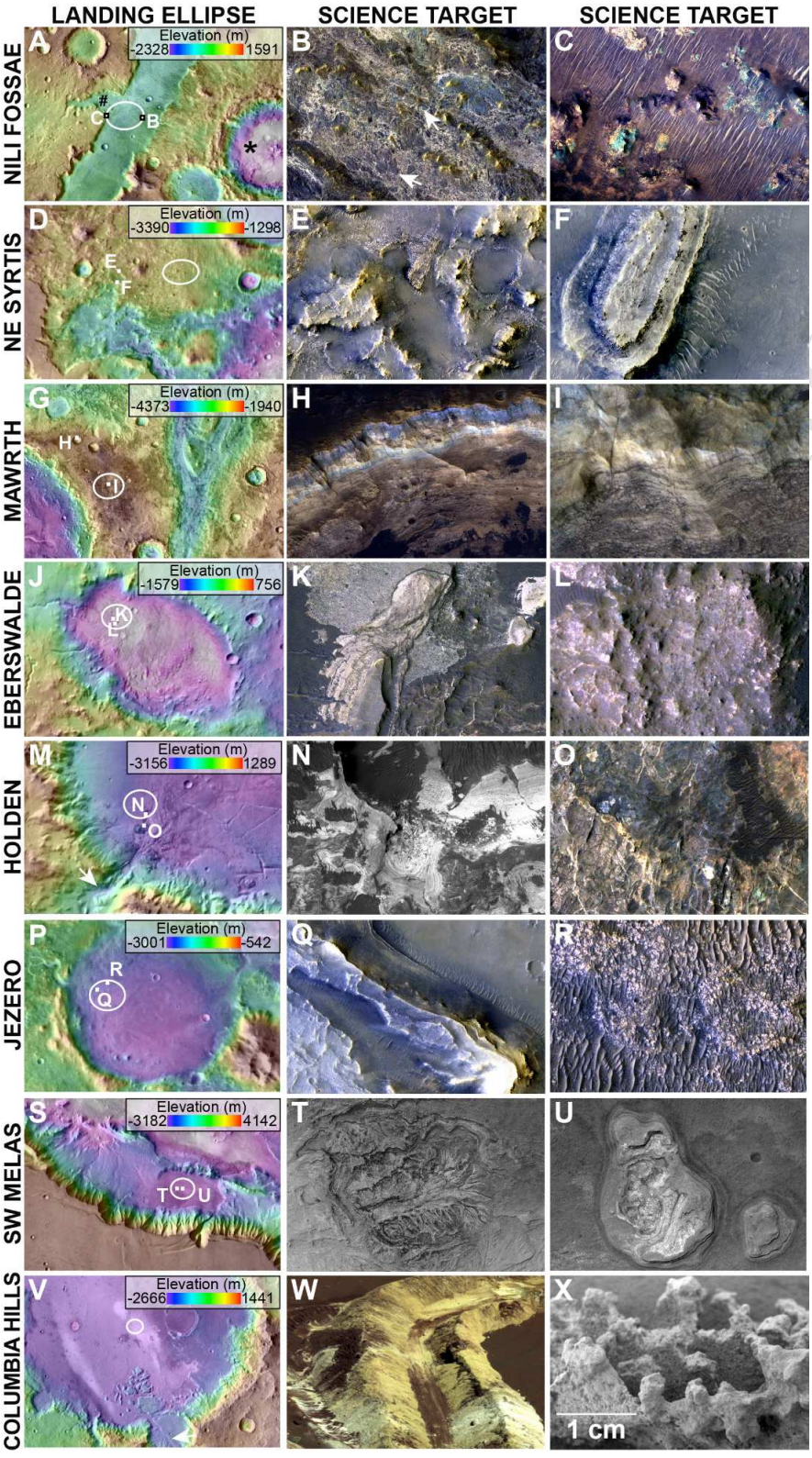

709

710 **Figure 2.** Final eight Mars 2020 candidate landing sites (left column, see Fig. 1 for context) and
711 primary science targets (middle and right columns) for each: Nili Fossae (A-C), NE Syrtis (D-F),
712 Mawrth Vallis (G-I), Eberswalde crater (J-L), Holden crater (M-O), Jezero crater (P-R), SW
713 Melas Basin (S-U), and Columbia Hills in Gusev crater (V-X). Left column shows MOLA
714 topography over THEMIS daytime images of candidate sites with approximate center and size of
715 the proposed landing ellipse (Table 9) and locations (white boxes) of high priority science targets
716 detailed in middle and right columns. North to top in all images and all HiRISE images are map
717 projected with a scale of 25 cm per pixel resolution. Nili Fossae: **A**) Nili Fossae is located west
718 of Hargraves crater ("*") and is a region rich in clays. White outline approximates the 9.7 km x
719 7.7 km landing ellipse centered at 21.0297°N, 74.3494°E. Scene is ~149 km across. **B**) Example
720 of Hargraves ejecta with brecciated rocks (e.g., white arrows). Image is ~487 m across. Subframe
721 of HiRISE IRB PSP_008716_2015. **C**) Diverse clays and other hydrated minerals on surfaces
722 adjacent to the trough may be accessible by the re-entrant valley ("#" in panel A). Image is ~712
723 m across. Subframe of HiRISE IRB PSP_003086_2015. NE Syrtis: **D**) NE Syrtis is located west
724 of the Isidis impact basin and southwest of Jezero crater, a region with Early Noachian bedrock
725 and diverse hydrated minerals. White outline approximates the 11.1 km x 8.2 km landing ellipse
726 centered 17.8899°N, 77.1599°E. Image is ~85.5 km across. **E**) Example diversity of hydrated
727 minerals within and outside the ellipse as indicated by CRISM include clays and carbonates.
728 Image is ~867 m across. Subframe of HiRISE IRB ESP_016443_1980. **F**) Mesas with CRISM-
729 detected carbonate signatures and layered rocks in stratigraphic sequence are found throughout
730 and outside of the ellipse. Image is ~695 m across. Subframe of HiRISE IRB
731 ESP_015942_1980. Mawrth Vallis (after Grant et al., 2010): **G**) Diverse mineralogy including
732 phyllosilicates and other hydrated mineral phases that may be consistent with multiple

depositional settings. White outline approximates the 11.9 km x 9.8 km landing ellipse centered 23.9685°N, -19.0609°E. Scene is ~118 km across. **H**) Northwest of the proposed landing ellipse, a sequence of Al-phyllosilicates (blue) over Fe/Mg phyllosilicates (varying shades of light brown) is well exposed and shows no evidence of inter-bedding and may record a complex aqueous alteration history. Image is ~1.2 km across. Subframe of HiRISE IRB PSP_004052_2045. **I**) Similar stratigraphy as seen outside the ellipse (H) is exposed in the wall of a small crater within the landing ellipse. Image is ~263 km across. Subframe of HiRISE IRB ESP_011884_2045. Eberswalde crater: **J**) Eberswalde is a 63 km-diameter crater northwest of Holden crater that hosted a paleolake. White outline approximates the 8.6 km x 7.7 km landing ellipse centered -23.7749°N, -33.5147°E. Scene is ~93 km across. **K**) Science targets include light-toned material (possible lacustrine and (or) bottomset beds), layered delta sediment, and giant white veins (lower middle). Scene is ~803 m across. Subframe of HiRISE IRB PSP_004000_1560. **L**) Large blocks visible within the Holden ejecta. Scene is ~365 m across. Subframe of HiRISE IRB ESP_012610_1560. Holden crater: **M**) Southwestern rim and floor of the 140 km-diameter Holden crater with rim breach from Uzboi Vallis (arrow). White outline approximates the 9.5 km x 8.1 km landing ellipse centered at -26.6130°N, -34.8167°E. Scene is ~83 km across. **N**) Example of finely layered, likely lacustrine and distal alluvial beds. Image is ~1 km across. Subframe of HiRISE RED ESP_028513_1530. **O**) Megabreccia in Holden. Image is ~605 m across. Subframe of HiRISE IRB color ESP_ 012320_1530. Jezero crater: **P**) Jezero is a ~49 km-diameter crater on the western margin of the Isidis impact basin that hosted a paleolake. White outline approximates the 10.7 km x 8.3 km landing ellipse centered at 18.4386°N, 77.5031°E. Scene is ~72 km across. **Q**) Eastern edge of main delta within the landing ellipse. Image is ~1.2 km wide. Subframe of HiRISE IRB ESP_046060_1985. **R**) Light-

toned, carbonate-bearing material may be lacustrine sediments or a regional carbonate-bearing unit. Image is ~312 m across. Subframe of HiRISE IRB PSP_002743_1985. SW Melas Basin: **S**) The basin perched on the southwestern rim of Melas Chasma in Valles Marineris hosted a paleolake. White outline approximates the 9.7 km x 8.7 km landing ellipse centered at -9.8132°N, -76.4679°E. Scene is ~115 km across. **T**) Deep subaqueous fans (Metz et al., 2009) visible through an erosional window in the center of the basin. Image is ~4.3 km across. Subframe of HiRISE PSP_007667_1700 RED. **U**) Example of a bright outcrop identified as hydrated silica (opal) of unknown origin (after Weitz et al., 2015; Williams and Weitz, 2014). Image is ~1.27 km across. Subframe of HiRISE ESP_044180_1700 RED. Columbia Hills: **V**) Southern rim and floor of the ~166 km-diameter Gusev crater with rim breach from Ma'adim Vallis (arrow). White outline approximates the 9.6 km x 8.7 km landing ellipse centered at -14.5510°N, 175.4527°E. Scene is ~150 km across. Both W and X are located inside the landing ellipse. **W**) Track near Tyrone Lowland created when the Spirit rover drove backwards and dragged right front wheel. The failed wheel plowed up deeper, yellowish salty soil beneath shallower, whitish salty soil. The two-layer soil structure (calcium sulfate–rich above, iron sulfate–rich below) reveals how the soils were deposited and how they interact with the Martian air. Subframe of a Spirit Pancam 3-frame mosaic from sol 788 taken on March 31, 2006. 753, 535, 432 nm (L257). NASA/JPL-Caltech/Cornell. For scale, the rover wheel track is ~12 cm across (crest to crest). **X**) Microscopic Imager view of silica formations taken by the Mars Exploration Rover Spirit near "Home Plate" in Gusev crater on Sol 1157. NASA/JPL-Caltech.

6. The Third Landing Site Workshop

The list of eight sites after the second community workshop was further culled to three at the end of the third community workshop held in Monrovia, CA February, 2017. Workshop participants included members of the science community, the RSSB, and the Mars 2020 Project and instrument science teams. The three-day meeting was very well attended, with more than 200 present and an additional ~50 remote participants each day. Remote attendees did not participate in the final assessment of the candidate landing sites.

At the start of the workshop, the Mars 2020 engineering teams summarized the outcome of their intensive studies of the landing and other hazards at each of the sites. The intent was to inform the science community that the TRN capability had been included in the baseline mission scenario, thereby enabling landing access to all of the remaining sites. Another objective was to provide the community with information regarding the methods used for assessing the landing sites, the maturity of the engineering assessment, and to summarize associated results for the candidate sites.

With respect to EDL, the 2020 Project found all eight final candidate sites possessed acceptable terrain properties for landing safely with no significant concerns. Potential issues related to atmospheric modeling were identified at the Columbia Hills, Mawrth Vallis, and SW Melas Basin sites. These issues could be addressed at the Columbia Hills and Mawrth Vallis sites by increasing the size of the landing ellipse to accommodate the greater uncertainty in the winds. Doing so had little impact on science potential of the two sites because the relatively benign nature of the surface terrain and distribution of ROIs at the sites suggested mission objectives could still be achieved. At the SW Melas Basin site, concerns related to atmospheric modeling uncertainties coupled with significant terrain hazards adjacent to the ellipse (due to the perched

nature of the site within the walls of the broader Melas Chasma) were less readily addressed, but not considered severe enough to warrant dropping the site from consideration.

With respect to the expected ability of the rover to traverse to ROIs after landing, the final eight sites fall into four main groups in terms of the necessary distance to be covered (Golombek et al., 2017). ROIs at Northeast Syrtis (primary ROIs in Noachian clay-bearing basement, carbonates and basalt cap) and Mawrth Vallis (primary ROIs in Noachian clays and fracture fills) are located close together, distributed across much of the ellipse, and require traverses of only ~4 km for access. Access to ROIs in Jezero crater (primary ROIs in delta deposits and basin fill carbonates) and Eberswalde crater (primary ROIs in delta deposits and Holden megabreccias) require traverses of ~8 km. Access to the distribution of ROIs in southwest Melas Chasma (delta and hydrated silica deposits) requires a ~6 km drive, whereas the ROIs in the Columbia Hills (silica deposits and Comanche carbonates) and Nili Fossae (Noachian-aged material in reentrant or valley and Hargraves crater ejecta) include one within and one outside their ellipse, thereby requiring ~12 km to be traversed and is the distance that can be accomplished in the nominal 2020 mission scenario. The ROIs in Holden crater (light-toned layered deposits and megabreccia) require a drive of ~16 km to reach because one (megabreccia) is south of the landing ellipse. In terms of the time needed to complete traverses to the ROIs at the various sites, NE Syrtis, Mawrth Vallis, and SW Melas Basin would have estimated traverse times of <50 sols, the traverse at Jezero crater and Eberswalde crater would require ~70 sols, Nili Fossae and the Columbia Hills traverse would last ~85 sols (duration equates to the nominal mission drive distance of ~12 km), and the traverse at Holden crater would require ~150 sols and would exceed the nominal mission drive time/distance.

822 The traverse time at Holden crater is complicated by the numerous ripples in the landing
823 ellipse. Both Nili Fossae and Holden have abundant eolian ripples, but their orientation at Nili
824 Fossae would allow the rover to readily traverse within troughs whereas a slower traverse is
825 anticipated due to crossing ripples at Holden. The Eberswalde crater site displays some areas
826 covered by a mantling unit with superposing ripples and local scarps on the delta that are a
827 concern, whereas the SW Melas Basin site possesses some local scarps that may comprise
828 hazards. Nevertheless, traversable routes around these potential hazards appear to exist at both
829 sites and may simply result in somewhat more time to reach desired ROIs after landing. By
830 contrast, the greater distance to the ROIs at the Holden crater site (the ellipse is located on
831 alluvial fans northwest of the light-toned layered rocks and megabreccia) coupled with the
832 necessity for numerous ripple crossings result in the longest traverse time.

833 When factored in to overall expected mission performance, which includes such
834 considerations as the number of analyses needed, thermal impacts on hardware and operations
835 due to latitude, and the additional time need to accomplish surface mission objectives, only the
836 Holden crater site had a baseline reference mission that was likely to exceed the nominal mission
837 duration of just over 800 sols. This result integrates primarily the effects of the seasonally more
838 extreme environment and time needed to travel from the ellipse to the ROIs (complicated by
839 distance and necessary ripple crossings). In summary, although certain sites have engineering
840 concerns deemed to present significant challenges to achieving full mission objectives, including
841 some atmospheric (e.g., SW Melas Basin) and traversability (Holden crater) issues, none of the
842 sites were found to possess unacceptable risk. Moreover, because all of the final eight sites have
843 <1% probability of failure on landing, down-selection to 3-4 sites for continued evaluation was
844 based on their science value rather than engineering or safety concerns (Golombek et al., 2017).

Because science merit rather than engineering or safety concerns became the driver for final landing site selection, the third workshop objective was strongly focused on discussion of the science merits of the eight candidate landing sites that remained under consideration. Specifically, the goal of the workshop was to seek community insight and assessment of the virtues, uncertainties, strengths, and weaknesses of each candidate landing site relative to five science criteria (Table 10) that were developed by the Mars 2020 LSWG and were endorsed by the Mars 2020 Project Science Group. Community voting on the five science criteria served as community input (along with other factors such as engineering, operations, planetary protection, and the potential for returned sample science discoveries) to the process by which three or four sites were selected for further consideration.

Table 10. Science criteria for assessing candidate Sites at third 2020 landing site workshop

Criterion 1	The site is an astrobiologically-relevant ancient environment and has geologic diversity that has the potential to yield fundamental scientific discoveries when it is a) characterized for the processes that formed and modified the geologic record; and b) subjected to astrobiologically-relevant investigations (e.g., assessment of habitability and biosignature preservation potential). (scoring: 1=lowest potential, 5=highest potential)
Criterion 2	A rigorously documented and returnable cache of rock and regolith samples assembled at this site has the potential to yield fundamental scientific discoveries if returned to Earth in the future. (scoring: 1=lowest potential, 5=highest potential)
Criterion 3	There is high confidence in the assumptions, evidence, and any interpretive models that support the assessments for Criteria 1 and 2 for this site. (scoring: 1=lowest confidence, 5=highest confidence)
Criterion 4	There is high confidence that the highest-science-value regions of interest at the site can be adequately investigated in pursuit of Criteria 1 and 2 within the prime mission. (scoring: 1=lowest confidence, 5=highest confidence)
Criterion 5	The site has high potential for significant water resources that may be of use for future exploration—whether in the form of water-rich hydrated minerals, ice/ice regolith or subsurface ice. (scoring: 1=lowest potential, 5=highest potential)

858 In developing the five criteria (Table 10), the 2020 Project recognized that the selection of a
859 landing site is complicated by differing and deeply held opinions grounded in personal
860 experience, scientific taste, and varying interpretations of existing data. Moreover, because Mars
861 2020 is the first step in a possible Mars sample return effort, the decision on which place to land
862 has important implications for future planetary exploration and the associated scientific results.
863 As such, the criteria were designed to be as simple as possible so that differing opinions could be
864 developed, communally explored, and recorded at the third workshop.

865 The community assessment was made using an online "ballot" submitted to Google Docs and
866 subsequently tabulated in near real-time. Workshop participants were instructed to assess each
867 site relative to each criterion (Table 10) using values of one (lowest) to five (highest). Criterion
868 five was considered less of a factor in assessing the sites and was not used as a primary factor in
869 distinguishing their merits. Summary results were presented as color plots with red (low), yellow
870 (intermediate), and green (high) portraying the average and standard deviation of each site
871 relative to individual criteria (Figure 3). Results were also presented as a summary of the average
872 score for all five criteria for each site (Figure 4). Although the standard deviation associated with
873 the ranking of each site relative to each criterion is significant (Figures 3 and 4), some broad
874 trends are discussed below.

875 The third workshop summary plots (Figures 3 and 4) relative to each criterion (Table 10)
876 revealed that the Jezero crater and NE Syrtis sites were consistently assessed higher for criteria
877 one and two (related to astrobiological relevance and potential of returned samples, respectively)
878 and were as high or nearly as highly ranked as other sites relative to criteria three and four
879 (related to confidence of site interpretations and accessibility of targets in ROIs, respectively).
880 By contrast, the Holden crater and SW Melas Basin sites were consistently assessed the lowest

881 relative to criteria one and two and were ranked lower or nearly as low as any other site relative
882 to criteria three and four (Figures 3 and 4).

883 Columbia Hills, Eberswalde crater, Mawrth Vallis, and Nili Fossae sites (Figures 3 and 4)
884 received an intermediate assessment relative to the aforementioned sites, and all received fairly
885 similar values for each criterion. The Nili Fossae site, however, was assessed slightly lower
886 relative to criteria one and four, and all four of these intermediate sites were ranked nearly the
887 same for criterion two. Eberswalde crater was assessed slightly higher for criterion three.

888 While the community assessment was being compiled, the LSWG and RSSB provided their
889 sense of the relative merits of the final eight sites. The timing of these presentations was
890 deliberate so as not to bias the community assessment. The LSWG was unanimous in their
891 opinion that Jezero should advance, and ≥75% of the group agreed that Mawrth and NE Syrtis
892 should also advance as final candidate sites. Jezero was favored because it is the oldest of the
893 deltaic sites and offers good access to a diversity of aqueous sedimentary facies, good evidence
894 for hydrous minerals and Fe/Mg carbonates in multiple configurations, and evidence for a
895 volcanic unit. Mawrth Vallis offers access to ancient Noachian rocks showing abundant evidence
896 for aqueous processes via extensive phyllosilicates, sulfates and hydrated silica that may be
897 related to impact-generated hydrothermalism, and a dark capping unit that may be igneous and
898 Hesperian-aged. Nevertheless, the depositional model is less well-understood than for other
899 dominantly sedimentary sites. Stratigraphy at NE Syrtis provides access to some of the oldest
900 rocks on Mars and spans the Pre-Noachian to Early Hesperian and allows tracking Mars
901 environmental change, sampling of multiple aqueous environments for biosignatures features,
902 includes three distinct igneous units, and displays intact Pre-Noachian strata in megabreccia
903 blocks.

The LSWG recommended the Columbia Hills and Holden sites should not advance to the final three. For Columbia Hills, the LSWG believed that investment of the Mars 2020 payload would not resolve the significant ambiguity regarding the geological context of lithologies of interest nor place significant new constraints on the potential biogenicity of the opaline silica deposits. For Holden, operational challenges were not viewed as being outweighed by the habitability, biosignature preservation potential or diversity of depositional environments likely present as compared to other potential landing sites. The remaining sites, Nili Fossae, Eberswalde, and SW Melas, were each evaluated to be of overall intermediate merit, but worthy of advancement by 20-40% of the LSWG.

The RSSB placed emphasis on candidate sites where the sample cache collected by the Mars 2020 rover was deemed of sufficient scientific value to merit returning. Accordingly, sites for which samples could present a strong potential for astrobiologically significant discoveries, advances in geochronology and martian petrogenesis, and significant increases in the understanding of Mars as a system were assessed the highest. Moreover, to minimize returnability risk, the RSSB felt the landing site should meet the needs of astrobiology and at least one significant geology objective. With this in mind, the RSSB developed preliminary rankings and assessed Jezero as likely yielding samples with the highest astrobiology potential and moderate to high geology and Mars system potential. Columbia Hills samples were viewed as having the highest overall potential for advances in geology with a medium to high astrobiology potential. Mawrth Vallis, Nili Fossae, and NE Syrtis were also viewed as yielding samples with a medium to high geology potential, but lesser astrobiology potential, especially for Nili Fossae and NE Syrtis. Eberswalde samples could be of medium value for assessing both

926 geology and astrobiology questions, whereas the value of samples from SW Melas and Holden
927 were rated the lowest in terms of both overall geology and astrobiology potential.

928 **Figure 3.**

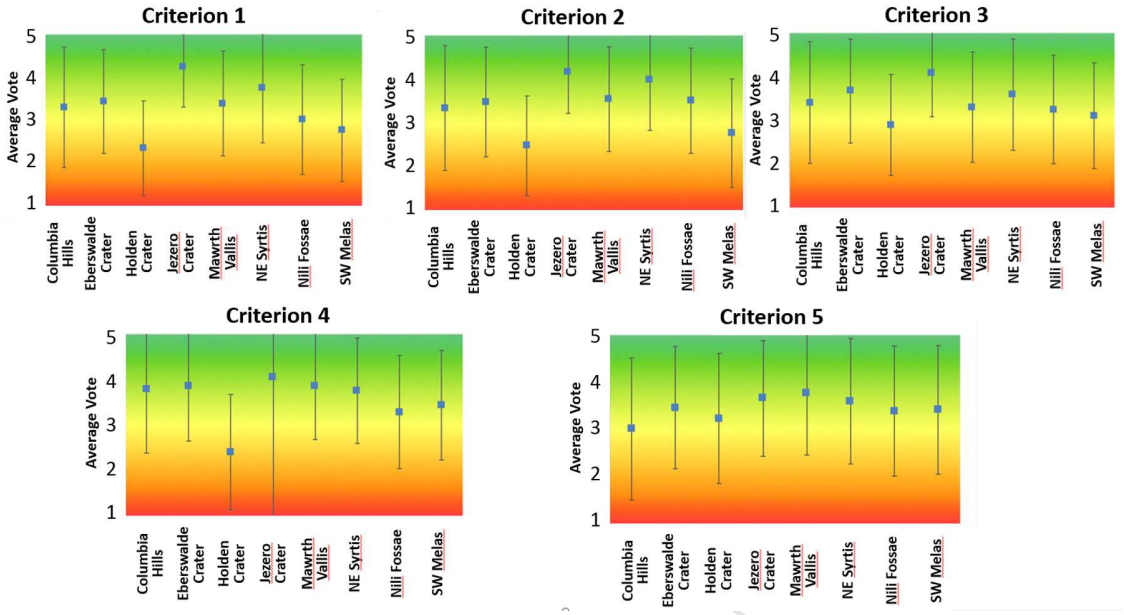

929

930

931 **Figure 3.** Summary assessment of all eight candidate sites (average) relative to each of the five
932 criteria considered at the third community workshop (Table 10). Red (1) is lowest, Yellow (3) is
933 intermediate, and Green (5) is high. Error bars reflect the standard deviation which is relatively
934 large compared to the difference between the responses for individual site, but enables general
935 statements regarding the assessment to be interpreted. For example, the NE Syrtis Major and
936 Jezero crater sites consistently are assessed to be of higher value relative to the criteria than the
937 Holden crater and southwest Melas Chasma sites (see text for discussion). The authors wish to
938 recognize Jacob Adler at ASU for his work in creating the assessment tool used for Workshop 3.

939

940 **Figure 4.**

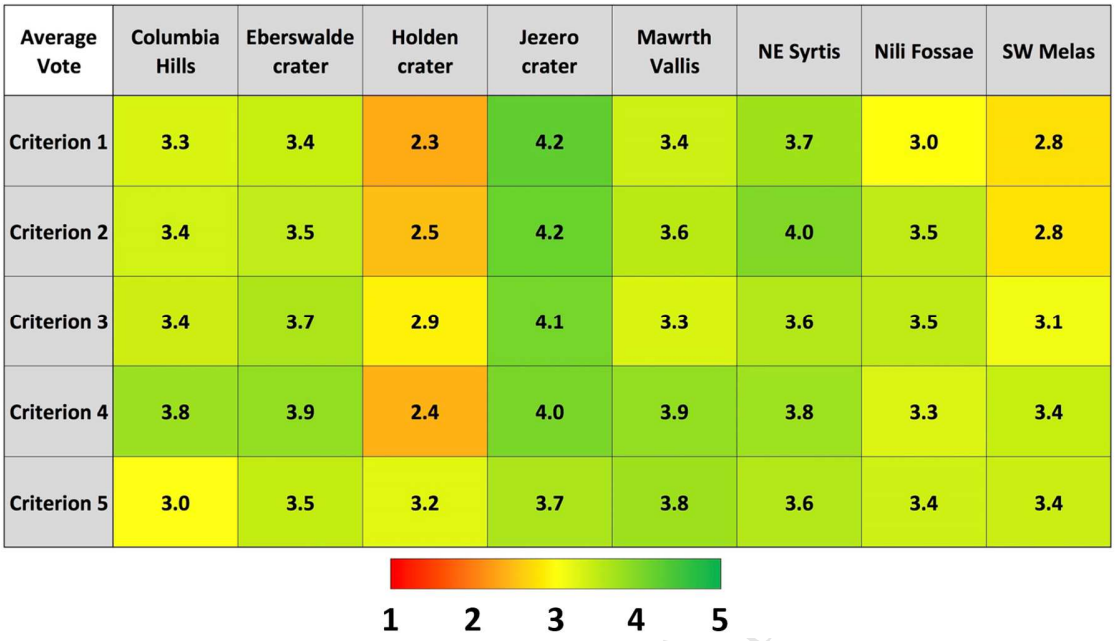

Average Vote	Columbia Hills	Eberswalde crater	Holden crater	Jezero crater	Mawrth Vallis	NE Syrtis	Nili Fossae	SW Melas
Criterion 1	3.3	3.4	2.3	4.2	3.4	3.7	3.0	2.8
Criterion 2	3.4	3.5	2.5	4.2	3.6	4.0	3.5	2.8
Criterion 3	3.4	3.7	2.9	4.1	3.3	3.6	3.5	3.1
Criterion 4	3.8	3.9	2.4	4.0	3.9	3.8	3.3	3.4
Criterion 5	3.0	3.5	3.2	3.7	3.8	3.6	3.4	3.4

941

942 **Figure 4.** Summary assessment using the average score for all five criteria for each site (Table
943 10). Red (1) is lowest, Yellow (3) is intermediate, and Green (5) is high. The NE Syrtis Major
944 and Jezero crater sites are consistently are assessed to be of higher value (more green) relative to
945 the criteria than the Holden crater and SW Melas Basin sites (more yellow and orange). The
946 Columbia Hills, Eberswalde crater, Marwth Vallis, and Nili Fossae sites were assessed to be
947 intermediate in value relative to the criteria (see text for discussion). The authors wish to
948 recognize Jacob Adler at ASU for his work in creating the assessment tool used for Workshop 3.

949

950 **7. Narrowing the List of Candidate Sites**

951 Following the third community workshop, the Mars Landing Site Steering Committee, the
952 Mars 2020 Project Science Group, representatives from the RSSB, and several Mars 2020
953 project engineers met to down-select the candidate sites. Key inputs that informed committee
954 deliberations included: the discussions and assessments from the workshop; project-internal

955 evaluations from the RSSB; project-internal evaluations from the Mars 2020 LSWG; and, for
956 some sites, engineering factors related to predicted operational efficiency.

957 It was noted that the Mars 2020 mission has a distinct and diverse set of goals centered on *in*
958 *situ* investigations, preparation of a scientifically worthy sample cache for possible Earth return,
959 seeking the signs of ancient life, and investigating nonbiological aspects of Mars geology,
960 climate, and planetary history. Accomplishing these objectives within the baseline ~800 sol
961 mission depends on the collective efficiency of engineering and science operations that include
962 drive distance, ease of traverse, temperature extremes, and time needed for *in situ* exploration.
963 Extreme high temperatures may also lead to some unknown amount of sample degradation as the
964 cache awaits potential Earth return on the Martian surface. With these factors in mind, all of the
965 sites were found to be very compelling candidate landing sites for the mission. Consideration of
966 specific aspects of each, however, allowed distinguishing between their overall merits with
967 respect to mission objectives.

968 The NE Syrtis site was ranked very highly by both the LSWG and by workshop attendees. A
969 key feature of NE Syrtis is the lithologic diversity that appears to span over a broad interval of
970 early Mars history, coupled with the clear and readily accessible stratigraphic context throughout
971 the landing ellipse. Units of scientific interest include large, well-exposed blocks of megabreccia
972 probably emplaced by the ~4 Ga Isidis impact, abundant phyllosilicates, and a high
973 concentration of carbonates that could harbor evidence of past climate and of possible life (e.g.
974 in an ancient, subsurface aquifer and serpentinizing system). A widespread mafic capping unit
975 present in the ellipse could provide important chronostratigraphic context, but only if determined
976 to be of igneous origin. Highly desirable Hesperian Syrtis lava flows and sulfates have been
977 identified at a distance of 20 to 30 km from the landing ellipse, but may lie beyond the range of

978 an extended mission. Nevertheless, the site was viewed more highly than most sites and on a par
979 with Jezero crater and was therefore selected as a final candidate site.

980 The Jezero crater site was strongly endorsed by the Mars 2020 LSWG, RSSB, and workshop
981 attendees. Jezero crater offers a well-defined delta environment including: the bottomset and
982 lacustrine facies deemed to be fine-grained and most favorable for organic concentration and
983 preservation; a large and geologically diverse headwaters region emptying into an open, deep
984 lake; and an intriguing carbonate-bearing unit that may preserve a record of the ancient Martian
985 carbon cycle (Edwards and Ehlmann, 2015). Jezero is clearly Noachian in age and the oldest of
986 the candidate crater paleolake sites considered (e.g., Fassett and Head, 2008b). On the negative
987 side, the mafic crater floor unit has a young age as estimated by crater counts and may only be of
988 Amazonian age (e.g., Schon et al., 2012). The floor unit lacks unambiguous evidence for a
989 volcanic origin and if it is not volcanic, the floor materials may have potentially limited
990 applicability for returned sample science aimed at constraining the Martian cratering record. The
991 positive attributes were viewed so highly, however, that the site was selected as a final candidate
992 for landing.

993 After considerable discussion, the Columbia Hills site was forwarded as a final candidate site
994 based on a range of potentially attractive targets for Mars 2020 to investigate. Most notable
995 among these is a silica-rich, putative hydrothermal sinter deposit that some scientists, by analogy
996 to Earth, suggest is an excellent target for seeking evidence of possible ancient Martian life. In
997 addition, the presence of a diverse suite of previously characterized volcanic rocks, which was
998 ranked highly by the RSSB, should be useful for returned sample studies. Considerable time in
999 the workshop was spent evaluating the evidence supporting a hot spring origin for the key target
1000 at this site, and whether a surface mission could adequately test the hypothesis. In the end, the

committee agreed to retain Columbia Hills as a final candidate landing site to allow the nascent understanding of its geologic setting to be further developed and tested, and to allow time for the 2020 Project to more deeply study the science value and potential engineering challenges of the site (including those associated with sampling and interrogating cm-scale putative sinter exposures with the drill). Unlike some other sites in the group of eight discussed at the workshop, it was believed by the representatives of the groups present at the meeting that important changes in the assessment of this site might emerge via ongoing studies. Absent such revision, however, the Columbia Hills site is relatively less favorable compared to the NE Syrtis and Jezero crater sites.

The paleolake in Eberswalde crater was found less compelling than the broadly similar, but significantly older, Jezero crater site. While Eberswalde crater offers an attractively compact distribution of scientific targets, the limited overall diversity of key exploration targets coupled with their likely Hesperian age (e.g., Rice et al., 2013), made the site less compelling from the perspectives of astrobiological potential and constraining early planetary evolution. Finally, due to its relatively high southern latitude location, the site suffers from seasonal temperature extremes that would reduce operational efficiency during exploration. Collectively, these aspects led to the site being dropped from consideration.

Mawrth Vallis is a compelling site due to the unique accumulation of phyllosilicates, and its great antiquity. Although this site was considered favorable by all groups, strong concerns were also raised about: the uncertain origin of the phyllosilicates; the strong dependence of the astrobiological relevance of the site on only some of the different models for phyllosilicate formation and alteration; and the perceived degree of difficulty that the science team would have in establishing a robust geologic context at the site during surface exploration. Taken together,

1024 these concerns were deemed important enough by the committee for the site to be dropped from
1025 further consideration.

1026 At the Nili Fossae site, the presence of an undisputed igneous unit that can be associated with
1027 lavas from the Syrtis Major volcanoes to the south was a strong advantage to the site. However,
1028 the astrobiological potential of the site was considered by the committee to be inferior relative to
1029 other potential landing sites, such as the nearby NE Syrtis and Jezero crater, and was therefore
1030 dropped from consideration.

1031 The Holden crater site was found to lack a diversity of compelling scientific targets relative
1032 to the other sites, especially when compared to the other sites boasting broadly similar paleolake
1033 settings. Although the megabreccia in Holden is diverse and likely enables access to Noachian or
1034 even older rocks, their context is poorly constrained. Moreover, lake beds and (or) distal fan
1035 deposits are constrained by the age of Holden to be no older than Early Hesperian and may more
1036 likely be Late Hesperian in age (e.g., Irwin et al., 2013), thereby potentially making them less
1037 appealing. Finally, the Holden crater site is also the most challenged by temperature extremes
1038 due to its relatively high southern latitude and the expectation of long traverse distances and
1039 times over potentially difficult terrain. Taken together, these attributes led Holden to be dropped
1040 from consideration.

1041 Like the Holden site, SW Melas Basin was determined to be inferior to broadly similar
1042 paleolake sites, largely due to lack of evidence for mineralogical and lithologic diversity (e.g.,
1043 absence of compelling, accessible igneous rocks). Melas is thought to be the youngest of the lake
1044 sites under consideration (e.g., Davis et al., 2017), which may make it less interesting from the
1045 perspectives of astrobiology and planetary evolution and so was dropped from further
1046 consideration.

The final three candidate Mars 2020 landing sites represent each of the three environments most commonly considered favorable for detecting possible ancient life on Mars: fine-grained sediments and chemical precipitates deposited in ancient lakes (Jezero), deep crustal settings in which water interacts with rock (NE Syrtis), and surficial hot springs (Columbia Hills).

8. Converging on the Final Mars 2020 Landing Site

At the time this paper was written in mid-2018, three final candidate landing sites are undergoing further evaluation with respect to their science potential, landing safety, traverseability and complexity of surface operations (e.g., the ability to acquire samples from Regions of Interest during the nominal mission). Additional orbital images are being acquired, primarily for potential extended mission exploration targets. Carefully registered image and topographic base maps are being constructed to support these studies (Williams et al., 2018). The fourth and final landing site workshop will be held in October 2018, where the three remaining sites will be further assessed against all existing and new data and interpretations relative to achieving mission objectives. New results related to analyses of the science potential of the sites as well as presentations on potential extended mission targets at each of the final sites are being encouraged. For example, a region approximately midway between the NE Syrtis and Jezero crater sites is being investigated by the Mars 2020 Project as a possible extended mission destination for either or as a primary landing site that would potentially enable an extended mission traverse into Jezero crater. The goal of such a locale/site would be to enhance mission science return by effectively enabling access to regions of interest associated with both the NE Syrtis and Jezero crater sites. Finally, the Mars 2020 Project will provide detailed mission scenarios for each site that includes discussion of potential exploration targets, observations, and

sampling strategies relative to mission goals and important Mars science described in the 2013-2022 Planetary Science Decadal Survey.

The community assessment of each site emerging from the workshop will be included in subsequent meetings along with input from other involved groups (e.g., LSWG) that will ultimately lead to convergence on a final candidate site. Post workshop meetings will involve multiple groups, likely including those involved in the post third workshop meeting. Once the Mars 2020 Project reaches a final site recommendation, the selection of the site will be made by Associate Administrator in the Science Mission Directorate at NASA, with the selection likely occurring at least one year before launch.

9. Acknowledgements

This work was supported by NASA and JPL under JPL subcontract 1442524 to John Grant. Part of the work in this paper was supported by the Mars Program Office and Mars 2020 Project at the Jet Propulsion Laboratory, California Institute of Technology, under a contract with the National Aeronautics and Space Administration. The authors thank Tim Goudge and an anonymous reviewer for comments that improved the manuscript.

10. References

Arvidson, R.E., Ruff, S., Morris, R.V., Ming, D.W., Crumpler, L.S., Yen, A., Squyres, S.W., Bell, III, J.F., Cabrol, N.A., Farrand, W., Gellert, R., Gorevan, S., Greenberger, R., Grant, J.A., Guinness, E.A., Herkenhoff, K.E., Johnson, J.R., Klingelhofer, G., Li, R., McCoy, T., Moersch, J., McSween, H.Y., Murchie, S., Want, A., Wiseman, S., Madsen, M.B., Goetz, W., 2008. Spirit Mars Exploration Rover mission to Gusev Crater, Columbia Hills:

1091 Mission overview and selected results from Backstay to Home Plate, J. Geophys. Res.,
1092 113, E12S33, doi:10.1029/2008JE003183.

1093 Bell, J.F., III, Wolff, M.J., Malin, M.C., Calvin, W.M., Cantor, B.A., Caplinger, M.A., Clancy,
1094 R.T., Edgett, K.S., Edwards, L.J., Fahle, J., Ghaemi, F., Haberle, R.M., Hale, A., James,
1095 P.B., Lee, S.W., McConnochie, T., Noe Dobrea, E., Ravine, M.A., Schaeffer, D.,
1096 Supulver, K.D., Thomas, P.C., 2009. Mars Reconnaissance Orbiter Mars Color Imager
1097 (MARCI): Instrument description, calibration, and performance, J. Geophys. Res., 114,
1098 E08S92, doi:10.1029/2008JE003315.

1099 Bernard, D.E., Farley, K.A., 2016. Mars 2020 Rover Mission Status in 2016, International
1100 Astronautical Conference, Guadalajara, Mexico, September, 2016. Reference #IAC-16-
1101 A3.3A.10, 6p.

1102 Bhattacharya, J.P., Payenberg, T.H.D., Lang, S.D., Bourke, M.C., 2005. Dynamic river channels
1103 suggest a long-lived Noachian crater lake. Geophys. Res. Lett., 32, L10201,
1104 doi:10.1029/2005GL022747.

1105 Bibring, J.-P., Soufflot, A., Berthé, M., Langevin, Y., Gondet, B., Drossart, P., Bouyé, M.,
1106 Combes, M., Puget, P., Semery, A., Bellucci, G., Formisano, V., Moroz, V., Kottsov, V.,
1107 Bonello, G., Erard, S., Forni, O., Gendrin, A., Manaud, N., Poulet, F., Poulleau, G.,
1108 Encrenaz, T., Fouchet, T., Melchiori, R., Altieri, F., Ignatiev, N., Titov, D., Zasova, L.,
1109 Coradini, A., Capacionni, F., Cerroni, P., Fonti, S., Mangold, N., Pinet, P., Schmitt, B.,
1110 Sotin, C., Hauber, E., Hoffmann, H., Jaumann, R., Keller, U., Arvidson, R., Mustard, J.,
1111 Forget, F., 2004. OMEGA: Observatoire pour la Minéralogie, l'Eau, les Glaces et
1112 l'Activité, in: Wilson A. (Ed.), Mars Express: The scientific payload. ESA SP-1240,
1113 Noordwijk, Netherlands: ESA Publications Division, ISBN 92-9092-556-6, pp. 37-49.

1114 Bibring, J.-P., Langevin, Y., Gendrin, A., Gondet, B., Poulet, F., Berthé, M., Soufflot, A.,
1115 Arvidson, R., Mangold, N., Mustard, J., Drossart, P., OMEGA team, 2005. Mars surface
1116 diversity as revealed by the OMEGA/Mars Express observations. Science, 307, 1576-
1117 1581.

1118 Bibring, J.-P., Langevin, Y., Mustard, J.F., Poulet, F., Arvidson, R., Gendrin, A., Gondet, B.,
1119 Mangold, N., Pinet, P., Forget, F., OMEGA team, 2006. Global mineralogical and aqueous
1120 Mars history derived from OMEGA/Mars Express data. Science, 312, 400-404, DOI:
1121 10.1126/science.1122659.

1122 Bishop, J.L., Noe Dobrea, E.Z., McKeown, N.K., Parente, M., Ehlmann, B.L., Michalski, J.R.,
1123 Milliken, R.E., Poulet, F., Swayze, G.A., Mustard, J.F., Murchie, S.L., Bibring, J.-P.,
1124 2008. Phyllosilicate diversity and past aqueous activity revealed at Mawrth Vallis, Mars.
1125 Science, 321, 830-833, DOI: 10.1126/science.1159699.

1126 Bishop, J.L., 2017. Seeking biosignatures on Mars today that are preserved from ancient
1127 evnironments at Mawrth Vallis: Lunar Planet. Sci. XLVIII, Abstract 3042, LPI, Houston,
1128 TX.

1129 Bramble, M.S., Mustard, J.F., Salvatore, M.R., 2017. The geological history of northeast Syrtis
1130 Major, Mars: Icarus, 293, 66-93, doi.org/10.1016/j.icarus.2017.03.030.

1131 Cabrol, N.A., Grin, E.A., 1999. Distribution, classification, and ages of Martian impact crater
1132 lakes, *Icarus*, v. *142*, p. 160-172.

1133 Cabrol, N.A., Grin, E.A, Dawidowicz, G., 1996. Ma'adim Vallis revisited through new
1134 topographic data: Evidence for an ancient intravalley lake, *Icarus*, v. 123, p. 269–283.

1135 Cabrol, N.A., Wynn-Williams, D.D., Crawford, D.A., Grin, E.A., 2001. Recent aqueous
1136 environments in Martian impact craters: An astrobiological perspective, *Icarus, v. 154*, p.
1137 98-112.

1138 Christensen, P.R., Jakosky, B.M., Kieffer, H.H., Malin, M.C., McSween, Jr., H.Y., Nealson, K.,
1139 Mehall, G.L., Silverman, S.H., Ferry, S., Caplinger, M., Ravine, M., 2004. The Thermal
1140 Emission Imaging System (THEMIS) for the Mars 2001 Odyssey Mission. Space Science
1141 Reviews, 110, 85-130.

1142 Coombs, A., 2016. Precision landing will be key to NASA's Mars 2020 rover, Eos, 97,
1143 https://doi.org/10.1029/2016EO056219.

1144 Davis, J.M., Grindrod, P.M., Williams, R.M.E., Fawdon, P., Gupta, S., Balme, M.R., 2017.
1145 Fluvial mapping and stratigraphy of the south-western Melas basin and plateau, Valles
1146 Marineris, Mars: Episodicfluvial phases and implications for climate: LPSC XLVIII,
1147 Abstract 1991. LPI, Houston, TX.

1148 Dromart, G., Quantin, C., Broucke, O., 2007. Stratigraphic architectures spotted in southern
1149 Melas Chasma, Vallis Marineris, Mars. Geology, 35(4), 363-366.

1150 Edgar, L.A., Skinner, J.A., 2016. 1:75K-scale mapping of southwestern Melas Chasma, Mars:
1151 LPSC XLVII, Abstract 7016. LPI, Houston, TX.

1152 Edwards, C.S., Ehlmann, B.L., 2015. Carbon sequestration on Mars: Geology, 43, 863–866,
1153 doi:10.1130/G36983.1.

1154 Ehlmann, B.L., Mustard, J.F., Fassett, C.I., Schon, S.C., Head III, J.W., Des Marais, D.J., Grant,
1155 J.A., Murchie, S.L., CRISM team, 2008a. Clay mineralogy and organic preservation

potential of lacustrine sediments from a Martian delta environment, Jezero crater, Nili Fossae, Mars. Nature Geoscience, 1, doi:10.1038/ngeo207.

Ehlmann, B.L., Mustard, J.F., Murchie, S.L., Poulet, F., Bishop, J.L., Brown, A.J., Calvin, W.M., Clark, R.N., Des Marias, D.J., Milliken, R.E., Roach, L.H., Roush, T.L., Swayze, G.A., Wray, J.J., 2008b. Orbital identification of carbonate-bearing rocks on Mars. Science, 322, 1828-1832, DOI: 10.1126/science.1164759.

Ehlmann, B.L., et al., 2009. Identification of hydrated silicate minerals on Mars using MRO-CRISM: Geologic context near Nili Fossae and implications for aqueous alteration, J. Geophys. Res., 114, E00D08, doi:10.1029/2009JE003339.

Ehlmann, B.L., Mustard, J.F., Swayze, G.A., Clark, R.N., Bishop, J.L., Poulet, F., Des Marais D.J., Roach, L.H., Milliken, R.E., Wray, J.J., Barnouin-Jha, O., Murchie, S.L., 2010. Identification of hydrated silicate minerals on Mars using MRO-CRISM: Geologic context near Nili Fossae and implications for aqueous alteration. J. Geophys. Res., 114, E00D08, doi:10.1029/2009JE003339.

Ehlmann, B.L., Mustard, J.F., 2012. An in-situ record of major environmental transitions on early Mars at Northeast Syrtis Major. Geophys. Res. Lett. 39. doi:10.1029/2012GL051594.

Farley, K.A., Williford, K.H., 2017. Seeking signs of life, and more: NASA's Mars 2020 mission, Eos, 98, https://doi.org/10.1029/2017EO066153.

Farmer, J., Des Marais, D., 1999. Exploring for a record of ancient Martian life. J. Geophys. Res., 104(E11), 26977-26995, doi:10.1029/1998JE000540.

1177 Fassett, C.I., Head, J.W., 2005. Fluvial sedimentary deposits on Mars: Ancient deltas in a crater
1178 lake in the Nili Fossae region. Geophys. Res. Letts., 32, L14201,
1179 doi:10.1029/2005GL023456.

1180 Fassett, C.I., Head J.W., 2008a. Valley network-fed, open-basin lakes on Mars: Distribution and
1181 implications for Noachian surface and subsurface hydrology, Icarus, 198, 37–56,
1182 doi:10.1016/j.icarus.2008.06.016.

1183 Fassett, C.I., Head J.W., 2008b. The timing of Martian valley network activity: Constraints from
1184 buffered crater counting, Icarus, 195, 61–89, doi:10.1016/j.icarus.2007.12.009.

1185 Frey, H., 2008. Ages of very large impact basins on Mars: Implications for the late heavy
1186 bombardment in the inner solar system: Geophys. Res. Letts, 35,
1187 doi:10.1029/2008GL033515.

1188 Frey, H.V., Frey, E.L., Hartmann, W.K., Tanaka, K.L.T., 2003. Evidence for buried “pre-
1189 Noachian” crust pre-dating the oldest observed surface units on Mars, Lunar Planet. Sci.
1190 Conf. XXXIV, Abstract 1848.

1191 Golombek, M.P., Grant, J.A., Parker, T.P., Kass, D.M., Crisp, J.A., Squyres, S.W., Haldemann,
1192 A.F.C., Adler, M., Lee, W., Bridges, N.T., Arvidson, R.E., Carr, M.H., Kirk, R.L.,
1193 Knocke, P.C., Roncoli, R.B., Weitz, C.M., Schofield, J.T., Zurek, R.W., Rice, J.W., 2003.
1194 Selection of the Mars Exploration Rover landing sites. J. Geophys. Res., 108, 8072, doi:
1195 10.1029/2003JE002074.

1196 Golombek, M.P., et al., 2006. Geology of the Gusev cratered plains from the Spirit rover
1197 transverse, J. Geophys. Res., 111, E02S07, doi:10.1029/2005JE002503.

1198 Golombek, M.P., Grant, J.A., Kipp, D., Vasavada, A., Kirk, R., Fergason, R., Bellutta, P., Calef,
1199 F., Larsen, K., Katayama, Y., Huertas, A., Beyer, R., Chen, A., Parker, T., Pollard, B.,
1200 Lee, S., Sun, Y., Hoover, R., Sladek, H., Grotzinger, J., Welch, R., Noe Dobrea, E.,
1201 Michalski, J., Watkins, M., 2012. Selection of the Mars Science Laboratory landing site,
1202 *Space Science Reviews,* 170, 641-737, doi:10.1007s11214-012SPAC875R1.

1203 Golombek, M.P., Grant, J.A., Farley, K.A., Chen, A., 2015. Science objectives, engineering
1204 constraints, and landing sites proposed for the Mars 2020 rover mission. Lunar Planet. Sci.
1205 XXXXVI, Abstract 1653, LPI, Houston, TX.

1206 Golombek, M.P., Grant, J.A., Farley, K.A., Williford, K., Chen, A., Otero, R.E., Ashley, J.W.,
1207 2016. Down-selection of landing sites proposed for the Mars 2020 mission. Lunar Planet.
1208 Sci. XXXXVII, Abstract 2324, LPI, Houston, TX.

1209 Golombek, M.P., Otero, R.E., Heverly, M.C., Ono, M., Williford, K.H., Rothrock, B.,
1210 Milkovich, S., Almeida, E., Calef, F., Williams, N., Ashley, J., Chen, A., 2017.
1211 Characterization of Mars Rover 2020 prospective landing sites leading up to the second
1212 down-selection: (expanded abstract): 48th Lunar and Planetary Science, Abstract #2333,
1213 Lunar and Planetary Institute, Houston.

1214 Golombek, M.P., Grant, J.A., Farley, K.A., Williford, K.H., Otero, R.E., Chen, A., 2018. Final
1215 three landing sites for the Mars 2020 rover: LPSC XLIX, abstract 2130, LPI, Houston, TX.

1216 Goudge, T.A., Head, J.W., Mustard, J.F., Fassett, C.I., 2012. An analysis of open-basin lake
1217 deposits on Mars: Evidence for the nature of associated lacustrine deposits and post-
1218 lacustrine modification processes, Icarus, 219, 211–229, doi: 10.1016/j.icarus.2012.02.027.

1219 Goudge, T.A., Mustard, J.F., Head, J.W., Fassett, C.I., Wiseman, S.M., 2015. Assessing the
1220 mineralogy of thewatershed and fan deposits of the Jezero crater paleolake system, Mars,
1221 J. Geophys. Res. Planets, 120,775–808, doi:10.1002/2014JE004782.

1222 Goudge, T. A.; Milliken, R. E.; Head, J. W.; Mustard, J. F.; Fassett, C. I., 2017a.
1223 Sedimentological evidence for a deltaic origin of the western fan deposit in Jezero crater,
1224 Mars and implications for future exploration, EPSL, 458, 357-365, doi:
1225 10.1016/j.epsl.2016.10.056.

1226 Goudge, T.A., Ehlmann, B.L., Fassett, C.I., Head, J.W., Mustard, J.F., Mangold, N., Gupta, S.,
1227 Milliken, R.E., Brown, A.J., 2017b. Jezero crater, Mars as a compelling site for future in
1228 situ exploration, LPSC XLVIII, Abstract 1197. LPI, Houston, TX.

1229 Grant, J.A., Golombek, M.P., Parker, T.J., Crisp, J.A., Squyres, S.W., Weitz, C.M., 2004.
1230 Selecting landing sites for the 2003 Mars Exploration Rovers. J. Planet. Space Sci., 52, 11-
1231 21.

1232 Grant, J.A., Wilson, S.A., Ruff, S.W., Golombek, M.P., Koestler, D.L., 2006. Distribution of
1233 rocks on the Gusev Plains and on Husband Hill, Mars, *Geophys. Res. Lett.*, 33, L16202,
1234 doi:10.1029/2006GL026964.

1235 Grant, J.A., Arvidson, R.E., Crumpler, L.S., Golombek, M.P., Hahn, B., Haldemann, A.F.C., Li,
1236 R., Soderblom, L.A., Squyres, S.W., Wright, S.P., Watters, W.A., 2006b. Crater gradation
1237 in Gusev crater and Meridiani Planum, Mars, *J. Geophys. Res.*, 111,
1238 doi:10.1029/2005JE002465.

1239 Grant, J.A., Irwin, III, R.P., Grotzinger, J.P., Milliken, R.E., Tornabene, L.L., McEwen, A.S.,
1240 Weitz, C.M., Squyres, S.W., Glotch, T.D., Thomson, B.J., 2008. HiRISE imaging of

impact megabreccia and sub-meter aqueous strata in Holden Crater, Mars. Geology, 36, 195-198, doi: 10.1130/G24340A.

Grant, J.A., Golombek, M.P., Grotzinger, J.P., Wilson, S.A., Watkins, M.M., Vasavada, A.R., Griffes, J.L., Parker, T.J., 2010a. The science process for selecting the landing site for the 2011 Mars Science Laboratory, *Planet. Space Sci.*, 59, 1114-1127, doi:10.1016/j.pss.2010.06.016.

Grant, J.A., Irwin, III, R.P., Wilson, S.A., 2010b. Chapter 12: Aqueous depositional settings in Holden crater, Mars, p. 323-346 *in* Cabrol, N.A., and E.A. Grin, (eds.) *Lakes on Mars*, Elsevier, Oxford, UK.

Grant, J.A., Irwin, III, R.P., Wilson, S.A., Buczkowski, D., Siebach, K., 2011. A lake in Uzboi Vallis and implications for late Noachian-Early Hesperian climate on Mars, *Icarus*, 212, 110-122, doi:10.1016/j.icarus.2010.11.024.

Grant, J.A., Wilson, S.A., 2012. A possible synoptic source of water for alluvial fan formation in southern Margaritifer Terra, Mars, *Planet. Space Sci.*, 72, 44-52, doi:10.1016/j.pss.2012.05.020.

Greeley, R., B. H. Foing, H. Y. McSween, G. Neukum, P. Pinet, M. van Kan, S. C. Werner, D. A. Williams, and T. E. Zegers (2005a), Fluid lava flows in Gusev crater, Mars, J. Geophys. Res., 110, E05008, doi:10.1029/ 2005JE002401.

Hiesinger, H., and J. W. Head III (2004), The Syrtis Major volcanic province, Mars: Synthesis from Mars Global Surveyor data, J. Geophys. Res., 109, E01004, doi:10.1029/2003JE002143.

1262 Irwin, R.P., Maxwell, T.A., Howard, A.D., Craddock, R.A., Leverington, D.W., 2002. A large
1263 paleolake basin at the head of Ma'adim Vallis, Mars, Science, 296, 2209 – 2212.

1264 Irwin, R.P., III, Grant, J.A., 2013. Geologic Map of MTM –15027, –20027, –25027, and –25032
1265 Quadrangles, Margaritifer Terra Region of Mars, *U.S. Geol. Surv.*, Scientific
1266 Investigations Map 3209.

1267 Irwin, R.P., III, Lewis, K.W., Howard, A.D., Grant, J.A., 2015. Paleohydrology of Eberswalde
1268 crater, Mars: *Geomorphology*, 240, 83-101.
1269 http://dx.doi.org/10.1016/j.geomorph.2014.10.012.

1270 Jaumann, R., Neukum, G., Behnke, T., Duxbury, T.C., Floohrer, J., Gasselt, S.V., Giese, B.,
1271 Gwinner, K., Hauber, E., Hoffmann, H., Hoffmeinster, A., Köhler, U., Matz, K.D.,
1272 McCord, T.B., Mertens, V., Oberst, J., Pischel, R., Rei, D., Ress, B., Roasch, T., Saiger,
1273 P., Scholten, F., Schwarz, O., Stephan, K., Wählisch, M., HRSC Co-Investigator Team,
1274 2007. The high resolution stereo camera (HRSC) experiment on Mars Express: Instrument
1275 aspects and experiment conduct from interplanetary cruise through the nominal mission.
1276 Planetary and Space Science, 55, 928-952, doi:10.1016/j.pss.2006.12.003.

1277 Jerolmack, D.J., Mohrig, D., Zuber, M.T., Byrne, S., 2004. A minimum time for the formation of
1278 Holden Northeast fan, Mars. Geophys. Res. Lett., 31, L21701,
1279 doi:10.1029/2004GL021326.

1280 Lewis, K.W., Aharonson, O., 2006. Stratigraphic analysis of the distributary fan in Eberswalde
1281 crater using stereo imagery. J. Geophys. Res., 111, E06001, doi: 10.1029/2005JE002555.

1282 Lewis, K.W., Aharonson, O., Grotzinger, J.P., Squyres, S.W., Bell III, J.F., Crumpler, L.S.,
1283 Schmidt, M.E., 2008. Structure and stratigraphy of Home Plate from the Spirit Mars
1284 Exploration Rover, J. Geophys. Res., 113, E12S36, doi:10.1029/2007JE003025.

1285 Loizeau, D., Mangold, N., Poulet, F., Bibring, J.-P., Gendrin, A., Ansan, V., Gomez, C., Gondet,
1286 B., Langevin, Y., Masson, P., Neukum, G., 2007. Phyllosilicates in the Mawrth Vallis
1287 region of Mars. J. Geophys. Res., 112, E08S08, doi:10.1029/2006JE002877.

1288 Loizeau, D., Mangold, N., Poulet, F., Ansan, V., Hauber, E., Bibring, J.-P., Gondet, B.,
1289 Langevin, Y., Masson, P., Neukum, G., 2010. Stratigraphy in the Mawrth Vallis region
1290 through OMEGA, HRSC color imagery and DTM. Icarus, 205, 396,
1291 doi:10.1016/j.icarus.2009.04.018.

1292 Loizeau, D., Werne, S.C., Mangold, N., Bibring, J.-P., and Vago, J.L., 2012. Chronology of
1293 deposition and alteration in the Mawrth Vallis region, Mars. Planet Space Sci 72:31–43.

1294 Loizeau, D., Mangold, N., Poulet, F., Bibring, J.-P., Bishop, J.L., Michalski, J., Quantin, C.,
1295 2015. History of the clay-rich unit at Mawrth Vallis, Mars: High-resolution mapping of a
1296 candidate landing site, J. Geophys. Res. Planets,120, 1820–1846,
1297 doi:10.1002/2015JE004894.

1298 Malin, M.C., Edgett, K.S., 2000. Evidence for recent groundwater seepage and surface runoff on
1299 Mars. Science, 288, 5475, 2230–2335, doi: 10.1126/science.288.5475.2330.

1300 Malin, M.C., Edgett, K.S., 2003. Evidence for persistent flow and aqueous sedimentation on
1301 Mars. Science, 302, 1931–1934, doi: 10.1126/science.10905444.

1302 Malin, M.C., Danielson, G.E., Ingersoll, A.P., Masursky, H., Veverka, J., Ravine, M.A.,
1303 Soulanille, T.A., 1992. Mars Observer Camera. J. Geophys. Res., 97, 7699–7718, doi:
1304 10.1029/92JE00340.

1305 Malin, M.C., Bell III, J.F., Cantor, B.A., Caplinger, M.A., Calvin, W.M., Clancy, R.T., Edgett,
1306 K.S., Edwards, L., Haberle, R.M., James, P.B., Lee, S.W., Ravine, M.A., Thomas, P.C.,

1307 Wolff, M.J., 2007. Context Camera investigation on board the Mars Reconnaissance
1308 Orbiter. J. Geophys. Res., 112, E05S04, doi: 10.1029/2006JE002808

1309 Mangold, N., Quantin, C., Ansan, V., Delacourt, C., and Allemand, P., 2004. Evidence for
1310 precipitation on Mars from dendritic valleys in the Valles Marineris area: Science, 305,
1311 78-81, doi:10.1126/science.1097549

1312 Mangold, N., Poulet, F., Mustard, J.F., Bibring, J.-P., Bondet, B., Langevin, Y., Ansan, V.,
1313 Masson, Ph., Fasset, C., Head, J.W., Hoffmann, H., Neukum, G., 2007. Mineralogy of the
1314 Nili Fossae region with OMEGA/Mars Express data: 2. Aqueous alteration of the crust. J.
1315 Geophys. Res. 112, E08S04. doi:10.1029/2006JE002835.

1316 Mangold, N., Kite, E.S., Kleinhans, M.G., Newsom, H., Ansan, V., Hauber, E., Kraal, E.,
1317 Quantin, C., Tanaka, K., 2012. The origin and timing of fluvial activity at Eberswalde
1318 crater, Mars. Icarus 220, 530–551. http://dx.doi.org/10.1016/j.icarus.2012.05.026.

1319 McCleese, D.J., Schofield, J.T., Taylor, F.W., Calcutt, S.B., Foote, M.C., Kass, D.M., Leovy,
1320 C.B., Paige, D.A., Read, P.L., Zurek, R.W., 2007. Mars Climate Sounder: An investigation
1321 of thermal and water vapor structure, dust and condensate distributions in the atmosphere,
1322 and energy balance of the polar regions, J. Geophys. Res., 112, E05S06,
1323 doi:10.1029/2006JE002790.

1324 McCoy, T.J., Sims, M., Schmidt, M.E., Edwards, L., Tornabene, L.L., Crumpler, L.S., Cohen,
1325 B.A., Soderblom, L.A., Blaney, D.L., Squyres, S.W., Arvidson, R.E., Rice, Jr., J.W.,
1326 Treguier, E., d'Uston, C., Grant, J.A., McSween, Jr., H.Y., Golombek, M.P., Haldemann,
1327 A.F.C., de Souza, Jr., P.A., 2008. Structure, stratigraphy, and origin of Husband Hill,
1328 Columbia Hills, Gusev Crater, Mars, *J. Geophys. Res*., 113, doi:10.1029/2007JE003041.

1329 McEwen, A.S., Eliason, E.M., Bergstrom, J.W., Bridges, N.T., Hansen, C.J., Delamere, W.A.,
1330 Grant, J.A., Gulick, V.C., Herkenhoff, K.E., Keszthelyi, L., Kirk, R.L., Mellon, M.T.,
1331 Squyres, S.W., Thomas, N., Weitz, C.M., 2007. Mars Reconnaissance Orbiter's High
1332 Resolution Imaging Science Experiment (HiRISE). J. Geophys. Res., 112, E05S02, doi:
1333 10.1029/2005JE002605.

1334 McEwen, A.S., Dundas, C.M., Mattson, S.S., Toigo, A.D., Ojha, L., Wray, J.L., Chojnacki, M.,
1335 Byrne, S., Murchie, S.L., Thomas, N., 2014. Nature Geoscience, 7, 53–58,
1336 doi:10.1038/ngeo2014.

1337 McLennan, S. M., M. A. Sephton, C. Allen, A.C. Allwood, R. Barbieri, D.W. Beaty, P. Boston,
1338 M. Carr, M. Grady, J. Grant, V. S. Heber, C. D. K. Herd, B. Hofmann, P. King, N.
1339 Mangold, G.G. Ori, A. P. Rossi, F. Raulin, S. W. Ruff, B. Sherwood Lollar, S. Symes, and
1340 M. G. Wilson (2012), Planning for Mars Returned Sample Science: Final report of the
1341 MSR End-to-End International Science Analysis Group (E2E-iSAG), Astrobiology, 12,
1342 175-230, doi: 10.1089/ast.2011.0805.

1343 McSween, H.Y., Arvidson, R.E, Bell III, J.F., Blaney, D., Cabrol, N.A, Christensen, P.R., Clark,
1344 B.C., Crisp, J.A., Crumpler, L.S., Des Marais, D.J., Farmer, J.D., Gellert, R., Ghosh, A.,
1345 Gorevan, S., Graff, T., Grant, J.A., Haskin, L.A., Herkenhoff, K.E., Johnson, J.R., Jolliff,
1346 B.L., Klingelhoefer, G., Knudson, A.T., McLennan, S, Milam, K.A., Moersch, R.V.,
1347 Morris, R.V., Rieder, R., Ruff, S.W., de Souza, Jr., P.A., Squyres, S.W., Wanke, H.,
1348 Wang, A., Wyatt, M.B., Yen, A., Zipfel, J., 2004. Basaltic rocks analyzed by the Spirit
1349 rover in Gusev Crater, *Science*, 305, 842-845, doi: 10.1126/science.3050842.

1350 Metz, J.M., Grotzinger, J.P., Mohrig, D., Milliken, R., Prather, B., Pirmez, C., McEwen A.S.,
1351 Weitz, C.M., 2009. Sublacustrine depositional fans in southwest Melas Chasma. J.
1352 Geophys. Res., 114, E10002, doi:10.1029/2009JE003365.

1353 Metz, J., Grotzinger, J., Okubo, C., Milliken, R., 2010. Thin□skinned deformation of
1354 sedimentary rocks in Valles Marineris, Mars, J. Geophys. Res., 115, E11004,
1355 doi:10.1029/2010JE003593.

1356 Michalski, J.R., Noe Dobrea, E.Z., 2007. Evidence for a sedimentary origin of clay minerals in
1357 the Mawrth Vallis region, Mars. Geology, 35, 830-833, doi: 10.1130/G23854A.1.

1358 Michalski, J., Poulet, F., Bibring, J.-P., Mangold, N., 2010. Analysis of phyllosilicate deposits in
1359 the Nili Fossae region of Mars: Comparison of TES and OMEGA data. Icarus, 206, 269-
1360 289, doi:10.1016/j.icarus.2009.09.006.

1361 Michalski, J., Cuadros, J., Niles, P., Parnell, J., Rogers A.D., Wright, S., 2013. Groundwater
1362 activity on Mars and implications for a deep biosphere, Nature Geoscience.
1363 10.1038/ngeo1706.

1364 Michalski, J.R., Onstott, T.C., Mojzsis, S.J., Mustard, J., Chan, Q.H.S., Niles, P.B., Johnson,
1365 S.S., 2017. The Martian subsurface as a potential window into the origin of life: Nature
1366 Geosci., 11, 21-26, doi:10.1038/s41561-017-0015-2.

1367 Milliken, R.E., Grotzinger, J., Grant, J.A., Arvidson, R., Murchie, S., 2008. Understanding
1368 sedimentary sources and sinks on Mars from orbit. Geol. Soc. Am. Prog. with Abs,
1369 Abstract 134-1.

1370 Milliken, R.E., Grotzinger, J.P., Thomson, B.J., 2010. Paleoclimate of Mars as captured by the
1371 stratigraphic record in Gale Crater. Geophys. Res. Lett., 37, L04201,
1372 doi:10.1029/2009GL041870.

1373 Milam, K.A., Stockstill, K.R., Moersch, J.E., McSween, H.Y., Tornabene, L.L., Ghosh, A.,
1374 Wyatt, M.B., Christensen, P.R., 2003. THEMIS characterization of the MER Gusev Crater
1375 landing site. J. Geophys. Res., 108, doi:10.1029/2002JE002023.

1376 Moore, J.F., Howard, A.D., Dietrich, W.D., Schenk, P.M., 2003. Martian layered fluvial
1377 deposits: implications for Noachian climate scenarios. Geophys. Res. Letts., 30, E06001.
1378 doi:10.1029/2003GL019002.

1379 Moore, J.M., Howard, A.D., 2005. Large alluvial fans on Mars. J. Geophys. Res., 110, E04005,
1380 doi:10.1029/2005JE002352.

1381 Murchie, S., Arvidson, R., Bedini, P. Beisser, K., Bibring, J.-P., Bishop, J., Boldt, J., Cavender,
1382 P., Choo, T., Clancy, R.T., Darlington, E.H., Des Marais, D., Espiritu, R., Fort, D., Green,
1383 R., Guinness, E., Hayes, J., Hash, C., Heffernan, K., Hemmler, J., Heyler, G., Humm, D.,
1384 Hutcheson, J., Izenberg, N., Lee, R., Lees, J., Lohr, D., Malaret, E., Martin, T., McGovern,
1385 J.A., McGuire, P., Morris, R., Mustard, J., Pelkey, S., Rhodes, E., Robinson, M., Roush,
1386 T., Schaefer, E., Seagrave, G., Seelos, F., Silverglate, P., Slavney, S., Smith, M., Shyong,
1387 W.-J., Strohbehn, K., Taylor, H., Thompson, P., Tossman, B., Wirzburger, M., Wolff, M.,
1388 2007. Compact Reconnaissance Imaging Spectrometer for Mars (CRISM) on Mars
1389 Reconnaissance Orbiter (MRO). J. Geophys. Res., 112, E05S03, doi:
1390 10.1029/2006JE002682.

1391 Mustard, J.F., Murchie, S.L., Pelkey, S.M., Ehlmann, B.L., Milliken, R.E., Grant, J.A., Bibring,
1392 J.-P., Poulet, F., Bishop, J., Noe Dobrea, E., Roach, L., Seelos, F., Arvidson, R.E.,

1393 Wiseman, S., Green, R., Hash, C., Humm, D., Malaret, E., McGovern, J.A., Seelos, K.,
1394 Clancy, T., Clark, R., Marais, D.D., Izenberg, N., Knudson, A., Langevin, Y., Martin, T.,
1395 McGuire, P., Morris, R., Robinson, M., Roush, T., Smith, M., Swayze, G., Taylor, H.,
1396 Titus, T., Wolff, M., 2008. Hydrated silicate minerals on Mars observed by the Mars
1397 Reconnaissance Orbiter CRISM instrument. Nature, 454, 305–309, doi:
1398 10.1038/nature07097.

1399 Mustard, J.F., Ehlmann, B.L., Murchie S.L., Poulet, F., Mangold, N., Head, J.W., Bibring, J.-P.,
1400 Roach, L.H., 2010. Composition, morphology, and stratigraphy of Noachian/Phyllosian
1401 crust around the Isidis Basin. J. Geophys. Res., 114, E00D12, doi:10.1029/2009JE003349.

1402 Mustard, J.F., Adler, M., Allwood, A., Bass, D.S., Beaty, D.W., Bell III, J.F., Brinckerhoff,
1403 W.B., Carr, M., Des Marais, D.J., Drake, B., Edgett, K.S., Eigenbrode, J., Elkins-Tanton,
1404 L.T., Grant, J.A., Milkovich, S.M., Ming, D., Moore, C., Murchie, S., Onstott, T.C., Ruff,
1405 S.W., Sephton, M.A., Steele, A., Treiman, A., 2013. Report of the Mars 2020 Science
1406 Definition Team, 154 pp., posted July, 2013, by the Mars Exploration Program Analysis
1407 Group (MEPAG) at
1408 http://mepag.jpl.nasa.gov/reports/MEP/Mars_2020_SDT_Report_Final.pdf.

1409 Mustard, J.F., Tarnas, J.D., 2017. Hydrogen production from the upper 15 km of Martian crust
1410 via Serpentinization: Implications for habitability: LPSC XLVIII, abstract 2384, LPI,
1411 Houston, TX.

1412 National Research Council, 2011. Vision and Voyages for Planetary Science in the Decade
1413 2013-2022: The National Academies Press, Washington, DC, 398 p.,
1414 https://doi.org/10.17226/13117.

1415 Noe Dobrea, E.Z., Bishop, J.L., McKeown, N.K., Fu, R,. Rossi, C., Heinlein, C., Hanus, V.,
1416 Michalski, J.R., Swayze, G., Poulet, F., Bibring, J.-P., Mustard, J.F., Ehlmann, B.L.,
1417 Arvidson, R., Morris, R.V., Murchie, S., McEwen, A.S., Malaret, E., Hash, C., CRISM
1418 Team, 2010. Mineralogy and stratigraphy of phyllosilicate-bearing and dark mantling units
1419 in the greater Mawrth Vallis/west Arabia Terra area: Constraints on geological origin. J.
1420 Geophys., Res., doi:10.1029/2009JE003351, in press.

1421 Osinski, G.R., Tornabene, L.L., Banerjee, N.R., Cockell, C.S., Flemming, R., Izawa, M.R.M.,
1422 McCutcheon, J., Parnell, J., Preston, L.J., Pickersgill, A.E., Pontefract, A., Sapers, H.M.,
1423 Southam, G., 2012. Impact-generated hydrothermal systems on Earth and Mars: Icarus,
1424 224, 347-363, doi.org/10.1016/j.icarus.2012.08.030

1425 Pondrelli, M., Baliva, A., Di Lorenzo, S., Marinangeli, L., Rossi, A.P., 2005. Complex evolution
1426 of paleolacustrine systems on Mars: An example from the Holden crater. J. Geophys. Res.,
1427 110, E04016, doi:10.1029/2004JE002335.

1428 Pondrelli, M.A., Rossi, A.P., Marinangeli, L., Hauber, E., Gwinner, K., Baliva, A., Di Lorenzo,
1429 S., 2008. Evolution and depositional environments of the Eberswalde fan delta, Mars.
1430 Icarus, 197, 429-451, doi:10.1016/j.icarus.2008.05.018.

1431 Poulet, F., Bibring, J.-P., Mustard, J.F., Gendrin, A., Mangold, N., Langevin, Y., Arvidson, R.E.,
1432 Gondet, B., Gomez, C., OMEGA Team, 2005. Phyllosilicates on Mars and implications
1433 for the early Mars history. Nature, 438, 623-628.

1434 Poulet, F., Gomez, C., Bibring, J.-P., Langevin, Y., Gondet, B., Pinet, P., Belluci, G., Mustard,
1435 J., 2007. Martian surface mineralogy from Observatoire pour la Minéralogie, l'Eau, les
1436 Glaces et l'Activité on board the Mars Express spacecraft (OMEGA/MEx): Global mineral
1437 maps. J. Geophys. Res., 112, E08S02, doi: 10.1029/2006JE002840.

1438 Quantin, C., Allemand, P., Mangold, N., Dromart, G., Delacourt, C., 2005. Fluvial and lacustrine
1439 activity on layered deposits in Melas Chasma, Valles Marineris, Mars. J. Geophys. Res.,
1440 110, E12S19, doi:10.1029/2005JE002440.

1441 Quinn, D. P., and Ehlmann, B. L., 2018, Water-lain sulfates and episodic fluvial sedimentation
1442 and erosion spanning the middle Noachian to Early Amazonian, Northeast Syrtis Major:
1443 LPSC XLIX, abstract 1840, LPI, Houston, TX.

1444 Rice, J. W., Jr., (2010), The Silica-Rich Hydrothermal Deposits of the Columbia Hills: A Key
1445 Candidate MAX-C Landing Site, Astrobiology Science Conference, Abstract 5618.

1446 Rice, M.S., Gupta, S., Bell III, J.F., Warner, N.H., 2011. Influence of fault-controlled topography
1447 on fluvio-deltaic sedimentary systems in Eberswalde crater, Mars. Geophys. Res. Lett. 38,
1448 L16203. http://dx.doi.org/10.1029/2011GL048149.

1449 Rice, M.S., Bell III, J.F., Gupta, S., Warner, N.H., Goddard, K., Anderson, R.B., 2013. A
1450 detailed geologic characterization of Eberswalde crater, Mars. Mars 8, 15–59.
1451 http://dx.doi.org/10.1555/mars.2013.0002.

1452 Ruff, S.W., Farmer, J.D., Calvin, W.M., Herkenhoff, K.E., Johnson, J.R., Morris, R.V., Rice,
1453 M.S., Arvidson, R.E., Bell, J.F., III, Christensen, P.R., Squyres, S.W., 2011.
1454 Characteristics, distribution, origin, and significance of opaline silica observed by the
1455 Spirit rover in Gusev crater, Mars, J. Geophys. Res., 116, doi:10.1029/2010JE003767.

1456 Ruff, S.W., Niles, P.B., Alfano, F., Clarke, A.B., 2014. Evidence for a Noachian-aged ephemeral
1457 lake in Gusev crater, Mars: Geology, 42, doi: 10.1130/G35508.1.

1458 Ruff, S.W., Farmer, J.D., 2016. Silica deposits on Mars with features resembling hot spring
1459 biosignatures at El Tatio in Chile; Nature Comm., 7, doi:10.1038/ncomms13554.

1460 Ruff, S.W., Farmer, J.D., Juarez Rivera, J., 2018. Testing alternative hypotheses for the origin of
1461 hydrothermal silica at Home Plate, Mars with implications for astrobiology: LPSC XLIX,
1462 abstract, LPI, Houston, TX

1463 Rummel, J.D., Beaty, D.W., Jones, M.A., Bakermans, C., Barlow, N.G., Boston, P.J., Chevrier,
1464 V.F., Clark, B.C., de Vera, J.-P.P., Gough, R.V., Hallsworth, J.E., Head, J.W., Hipkin,
1465 V.J., Kieft, T.L., McEwen, A.S., Mellon, M.T., Mikucki, J.A., Nicholson, W.L., Omelon,
1466 C.R., Peterson, R., Roden, E.E., Sherwood Lollar, B., Tanaka, K.L., Viola, D., Wray, J.J.,
1467 2014. A new analysis of Mars "Special Regions": Findings of the Second MEPAG Special
1468 Regions Science Analysis Group (SR-SAG2). Astrobiology, 14(11), p. 887-968,
1469 doi:10.1089/ast.2014.1227.

1470 Ryan, C.H., Tornabene, L.L., Cannon, K.M., Mustard, J.F., Sapers, H.M., Osinski, G.R., 2017.
1471 Geomorphological mapping of Hargraves ejecta in the Nili Fossae Trough: Insight into
1472 impact processes at potential Mars 2020 landing site: LPSC XLVIII, abstract 2861, LPI,
1473 Houston, TX.

1474 Salvatore, M. R., Goudge, T. A., Bramble, M. S., Edwards, C. S., Bandfield, J. L., Amador, E.
1475 S., Mustard, J. F., and Christensen, P. R., 2018, Bulk mineralogy of the NE Syrtis and
1476 Jezero craer regions of Mars derived through thermal infrared spectral analyses: Icarus,
1477 301, 76-96, doi.org/10.1016/j.icarus.2017.09.019.

1478 Saunders, S.R., 1979. Geologic map of the Margaritifer Sinus quadrangle of Mars, U.S. Geol.
1479 Surv. Misc. Invest. Ser. Map I–1144, scale 1:5M.

1480 Schon, S.C., Head, J.W., Fassett, C.I., 2012. An overfilled lacustrine system and prgradational
1481 delta in Jezero crater, Mars: Implications for Noachian climate: Planeatary and Space
1482 Science, 67, 28-45, doi:10.1016/j.pss.2012.02.003.

1483 Schultz, P.H., Schultz, R.A., Rogers, J., 1982. The structure and evolution of ancient impact
1484 basins on Mars. J. Geophys. Res. 87, 9803–9820.

1485 Scott, D.H., Tanaka, K.L., 1986. Geologic map of the western equatorial region of Mars. U. S.
1486 Geological Survey Miscellaneous Investigations Series I-1802-A, scale 1:15,000,000.

1487 Sherwood Lollar, B., Onstott, T.C., Lacrampe-Couloume, G., Ballentine, C.J., 2014. The
1488 contribution of the Precambrian continental lithosphere to global H2 production. Nature
1489 516 (7531): 379-382.

1490 Shotwell, R., Hays, L.E., Beaty, D.W., Goreva, Y., Kieft, T.L., Mellon, M.T., Moridis, G.,
1491 Peterson, L., Spycher, N., 2017. The potential for the off-nominal landing of an RTG-
1492 powered spacecraft on Mars to induce and artificial special region. Astrobiology (in
1493 review).

1494 Squyres, S.W., Arvidson, R.E., Bell, III, J.F., Bruckner, J., Cabrol, N.A., Calvin, W., Carr, M.H.,
1495 Christensen, P.R., Clark, B.C., Crumpler, L., Des Marais, D.J., d'Uston, C., Economou, T.,
1496 Farmer, J., Farrand, W., Folkner, W., Golombek, M., Gorevan, S., Grant, J.A., Greeley, R.,
1497 Grotzinger, J., Haskin, L., Herkenhoff, K.E., Hviid, S., Johnson, J., Klingelhofer, G.,
1498 Knoll, A.H., Landis, G., Lemmon, M.., Li, R., Madsen, M.B., Malin, M.C., McLennan,
1499 S.M., McSween, H.Y, Ming, D.W., Moersch, J., Morris, R.V., Parker, T., Rice, Jr., J.W.,
1500 Richter, L., Rieder, R., Sims, M., Smith, M., Smith, P., Soderblom, L.A., Sullivan, R.,
1501 Wanke, H., T. Wdowiak, H., Wolff, M., Yen, A., 2004. The Spirit rover's Athena science
1502 investigation at Gusev Crater, Mars, *Science*, 305, 794-799, doi: 10.1126/science.3050794.

1503 Squyres, S. W., et al., 2006. Rocks of the Columbia Hills, J. Geophys. Res., 111, E02S11,
1504 doi:10.1029/2005JE002562.

1505 Squyres, S. W., Aharonson, O., Clark, B. C., Cohen, B., Crumpler, L., de Souza, P. A., Farrand,
1506 W. H., Gellert, R., Grant, J., Grotzinger, J.P., Haldemann, A., Johnson, J. R., Klingelhöfer,
1507 G., Lewis, K., Li, R., McCoy, T., McEwen, A.S., McSween, H.Y., Ming, D.W., Moore, J.,
1508 Morris, R.V., Parker, T.J., Rice, J., Ruff, S., Schmidt, M., Schröder, C., Soderblom, L.A.,
1509 Yen, A., 2007. Pyroclastic activity at Home Plate in Gusev Crater, Mars, Science, 316,
1510 738-742, doi: 10.1126/science.1139045.

1511 Squyres, S. W., Arvidson R. E., Ruff, S., Gellert, R., Morris, R. V., Ming, D. W., Crumpler, L.,
1512 Farmer J. D., Des Marais, D. J., Yen, A., McLennan, S. M., Calvin, W., Bell, J. F., III,
1513 Clark, B. C., Wang, A., McCoy, T. J., Schmidt, M. E., de Souza, P. A., Jr, 2008. Detection
1514 of silica-rich deposits on Mars: Science, 320, 1063-1067, doi:10.1126/science.1155429.

1515 Summons, R.E., Amend, J.P., Bish, D., Buick, R., Cody, G.D., Des Marais, D.J., Dromart, G.,
1516 Eigenbrode, J.L., Knoll, A.H., Sumner, D.Y., 2010. Preservation of Martian organic and
1517 environmental records. Posted April, 2010, by the Mars Exploration Program Analysis
1518 Group (MEPAG) at http://mepag.jpl.nasa.gov/reports/.

1519 Weitz, C. M., Noe Dobrea, E., Wray, J. J., 2015. Mixtures of clays and sulfates within deposits
1520 in western Melas Chasma, Mars: Icarus, 251, 291-314, doi:10.1016/j.icarus.2014.04.009

1521 Williams, R. M. E., Weitz, C. M., 2014. Reconstructing the aqueous history within the
1522 southwestern Melas basin, Mars: Clues from stratigraphic and morphometric analyses of fans:
1523 Icarus, 242, 19-37, doi/10.1016/j.icarus.2014.06.030.

1524 Williams N.R., Lethcoe, H.A., Berger, L.M., Trautman, M.R., Fergason, R.L., Otereo, R.E.,
1525 Golombek, M.P., 2018. Controlled basemaps for Mars 2020 rover candidate landing sites. 49th
1526 Lunar and Planetary Science, Abstract #2799, Lunar and Planetary Institute, Houston.

1527 Wray, J.J., Ehlmann, B.L., Squyres, S.W., Mustard, J.F., Kirk, R.L., 2008. Compositional

1528 stratigraphy of clay-bearing layered deposits at Mawrth Vallis, Mars. Geophys. Res. Lett. 35,
1529 L12202.
1530 Zuber, M., Smith, D., Solomon, S., Muhleman, D., Head, J., Garvin, J., Abshire, J., Bufton, J.,
1531 1992. The Mars Observer Laser Altimeter Investigation. J. Geophys. Res., 97(E5), 7781-7797.

Highlights:

- Describes the science process for selecting the Mars 2020 rover landing site
- Down selection based on science merit rather than engineering constraints
- Over 30 candidate sites were narrowed to 3 finalists over three workshops
- Final candidate sites include Columbia Hills, Jezero crater, and NE Syrtis